



THE UNIVERSITY *of* EDINBURGH

Edinburgh Research Explorer

Evolution of a supergene that regulates a trans-species social polymorphism

Citation for published version:

Zheng, Y, Martin, S, Gotzek, D, Arsenault, SV, Duchon, P, Helleu, Q, Riba-Grognuz, O, Hunt, BG, Salamin, N, DeWayne, S, Ross, KG & Keller, L 2020, 'Evolution of a supergene that regulates a trans-species social polymorphism', *Nature Ecology & Evolution*. <https://doi.org/10.1038/s41559-019-1081-1>

Digital Object Identifier (DOI):

[10.1038/s41559-019-1081-1](https://doi.org/10.1038/s41559-019-1081-1)

Link:

[Link to publication record in Edinburgh Research Explorer](#)

Document Version:

Peer reviewed version

Published In:

Nature Ecology & Evolution

General rights

Copyright for the publications made accessible via the Edinburgh Research Explorer is retained by the author(s) and / or other copyright owners and it is a condition of accessing these publications that users recognise and abide by the legal requirements associated with these rights.

Take down policy

The University of Edinburgh has made every reasonable effort to ensure that Edinburgh Research Explorer content complies with UK legislation. If you believe that the public display of this file breaches copyright please contact openaccess@ed.ac.uk providing details, and we will remove access to the work immediately and investigate your claim.



Evolution of a Supergene That Regulates a Trans-Species Social Polymorphism

Zheng Yan¹, Simon H. Martin², Dietrich Gotzek³, Samuel V. Arsenault⁴, Pablo Duchén⁵, Quentin Helleu¹, Oksana Riba-Grognuz¹, Brendan G. Hunt⁴, Nicolas Salamin⁵, DeWayne Shoemaker⁶, Kenneth G. Ross⁴ and Laurent Keller¹

¹Department of Ecology and Evolution, University of Lausanne, Lausanne, Switzerland; ²Institute of Evolutionary Biology, the University of Edinburgh, UK
³Department of Entomology & Laboratories of Analytical Biology, National Museum of Natural History, Smithsonian Institution, Washington DC, USA; ⁴Department of Entomology, University of Georgia, Athens, GA, USA; ⁵Department of Computational Biology, University of Lausanne, Lausanne, Switzerland; ⁶Department of Entomology and Plant Pathology, University of Tennessee, Knoxville, TN, USA;

Correspondence: Laurent Keller, Department of Ecology and Evolution, University of Lausanne, Lausanne, CH-1015, Switzerland and Kenneth Ross, Department of Entomology, University of Georgia, Athens, GA, USA

E-mail: kenross@uga.edu, Laurent.keller@unil.ch

Supergenes are clusters of linked genetic loci that jointly affect the expression of complex phenotypes, such as social organisation. Little is known about the origin and evolution of these intriguing genomic elements. Here we analyse whole-genome sequences of males from native populations of six fire ant species and show that variation in social organisation is under the control of a novel supergene haplotype (termed *Sb*), which evolved by sequential incorporation of three inversions spanning half of a “social chromosome.” Two of the inversions interrupt protein-coding genes, resulting in the increased expression of one gene and modest truncation in the primary protein structure of another. All six socially polymorphic species studied harbour the same three inversions, with the single origin of the supergene in their common ancestor inferred by phylogenomic analyses to have occurred half a million years ago. The persistence of *Sb* along with the ancestral *SB* haplotype through multiple speciation events provides a striking example of a functionally important trans-species social polymorphism presumably maintained by balancing selection. We found that while recombination between the *Sb* and *SB* haplotypes is severely restricted in all species, a low level of gene flux between the haplotypes has occurred following the appearance of the inversions, potentially mitigating the evolutionary degeneration expected at genomic regions that cannot freely recombine. These results provide a detailed picture of the structural genomic innovations involved in formation of a supergene controlling a complex social phenotype.

While it is becoming increasingly clear that many animal species exhibit variation in social organisation, the underlying causes are rarely understood. The first discovery of a genetic basis for such variation was in the fire ant *Solenopsis invicta*^{1,2}. In this species, variation at a genomic region containing the odorant-binding protein gene *Gp-9* determines whether colonies contain just one (monogyne social form) or multiple (polygyne form) queens^{2,3}, a fundamental distinction associated with a suite of other important individual- and colony-level phenotypic differences⁴. Studies of invasive USA populations revealed that *Gp-9* is located in a supergene on the “social chromosome” (chromosome 16), and that the *Social b* (*Sb*) haplotype harbouring the *Gp-9^b* allele apparently does not recombine with the *Social B* (*SB*) haplotype containing the alternate *Gp-9^B* allele⁵. In the USA, monogyne colonies invariably contain a single homozygous *SB/SB* queen and only *SB/SB* workers, while polygyne colonies always contain multiple heterozygous (*SB/Sb*) queens together with predominantly *SB/Sb* and *SB/SB* workers (*Sb/Sb* females have low viability and *SB/SB* queens are killed by nestmate workers in polygyne colonies^{4,6}).

69 Reconstruction of the routes of supergene evolution is a longstanding goal with
70 important implications for our understanding of how these remarkable genomic
71 entities come to regulate the myriad features of complex phenotypes⁷⁻¹⁰. We
72 conducted a comparative genomic study of several fire ant species sampled from their
73 native ranges in order to characterize fully variation at the fire ant supergene and,
74 thereby, elucidate its origin and subsequent evolution.

75

76 **Results and Discussion**

77 A previous study showed that the supergene in *S. invicta* contains two inversions,
78 with a third one suggested by the fact that strong linkage extends approximately 1 Mb
79 beyond the two identified inversions¹¹. To test this prediction and characterize all of
80 the inversion breakpoints, we assembled new genomes of two *S. invicta* males (ant
81 males are haploid), one *Sb* and one *SB* male from the same polygyne colony from the
82 USA, using long (>10 Kb) PacBio sequence reads. Pairwise alignment of these two
83 newly assembled genomes revealed no sign of structural rearrangements at 15 of the
84 chromosomes (Extended Data Fig.1) but did reveal three large inversions in the *Sb*
85 haplotype which, collectively, span ~11.4 Mb of chromosome 16 (Fig. 1a).

86 The largest inversion, *In(16)I* (9.48 Mb), contains 476 annotated protein-coding
87 genes (Supplementary Table 1), including *Gp-9*. The proximal breakpoint disrupts a
88 “*F-box/WD repeat-containing protein 4-like*” gene (*FBXW4*; LOC105199310) 6nt
89 downstream from its start codon and 26nt downstream from the *SB* transcript start
90 site. The distal breakpoint disrupts a “*Phosphoglycerate mutase 2*” gene (*PGAM2*;
91 LOC105193833) 8nt downstream from the *SB* transcript start site in its 5’ UTR (Fig.
92 1b, see also Extended Data Fig. 2a-c). Remarkably, comparative RNA-seq analyses
93 show that neither of these genes exhibits consistent differential expression between
94 adults (males, queens, and workers) with alternate supergene haplotypes/genotypes
95 (all FDR $P > 0.05$ except for one sample type in one gene; Fig. 2), suggesting
96 minimal position effects of *In(16)I* in the regulation of proximal loci. In the case of
97 *FBXW4*, which likely plays a role in protein degradation¹² (Extended Data Fig. 3), the
98 *Sb* allele retains only the second in-frame start codon of the *SB* transcript, which is
99 seven codons downstream of the first annotated *SB* start codon. Modest truncation of

100 the *Sb* protein product, through use of this alternative translation start site, could
101 feasibly affect its function. However, *SB* translation initiation at the first *FBXW4* start
102 codon has yet to be demonstrated, so different-size proteins encoded by the alternate
103 alleles is not assured.

104 The second inversion, *In(16)2* (0.84 Mb), contains 46 annotated protein-coding genes
105 (Supplementary Table 2) and overlaps slightly with the first inversion, leading to a
106 short (586nt) doubly inverted fragment (Fig 1b; Extended Data Fig. 2d). Notably,
107 homologous copies of a “*Jockey-like mobile element*” are present at each breakpoint
108 of inversion *In(16)2*, suggesting that activity of this element promoted the appearance
109 of the inversion via ectopic (non-allelic homologous) recombination¹³ (Extended
110 Data Fig. 2e). The distal breakpoint of this inversion disrupts an uncharacterized gene
111 (LOC105193832) 75nt downstream of the *SB* transcript start site in its 5’ UTR
112 (Extended Data Fig. 2f). This uncharacterized locus exhibits significant differential
113 expression between individuals with alternate supergene haplotypes/genotypes in all
114 three castes according to RNA-seq analyses (FDR $P < 0.05$, Fig. 2), indicating a
115 widespread position effect of *In(16)2* on transcription of LOC105193832. The near-
116 constitutive nature of this effect is reinforced by consistently higher expression in
117 adults bearing the *Sb* haplotype for males (whole bodies), queens (1 of 2 tissues), and
118 workers (both tissues) (Fig. 2). Thus, somewhat surprisingly given that the breakpoint
119 interrupts the first exon of this gene, the effect is not degenerative; instead, *In(16)2*
120 generally enhances the gene’s transcription. This could be explained by the presence
121 of different promoter sequences at LOC105193832 in the *SB* and *Sb* haplotypes or by
122 differences in mRNA stability arising from their distinct 5’ UTR sequences. In further
123 support of this proposed upregulation of the *Sb* haplotype at LOC105193832, we
124 found significantly elevated *Sb* haplotype-specific expression at SNPs diagnostic for
125 the alternate *S. invicta* haplotypes in *SB/Sb* workers and queens (Supplementary Table
126 3). These striking patterns raise the possibility that *In(16)2* directly influences trait
127 variation relevant to social organization by altering LOC105193832 expression
128 patterns¹¹.

129 The third inversion, *In(16)3* (1.07 Mb), contains 27 protein-coding genes
130 (Supplementary Table 4), none of which is interrupted. The inversion does, however,
131 bridge the region between the centromere (enriched with satellite DNA repeats¹⁴) and

132 the two other inversions (Fig. 1b), thereby considerably expanding the region of
133 restricted recombination¹⁵ (centromeres typically exhibit reduced
134 recombination^{8,14,16}). The two breakpoints of *In(16)3* are in regions with similar
135 tandem repeat structures (Extended Data Fig. 2g-i), suggesting that this inversion also
136 originated by ectopic recombination¹³.

137 The results above expand upon the recent findings of Huang et al.¹¹ in several
138 important respects. First, we confirmed the predicted third supergene inversion
139 (*In(16)3*), the existence of which expands the conceived supergene boundaries into an
140 enlarged region of suppressed recombination (see Fig. 1b and LD results below).
141 Second, we were able to generate upgraded inventories of the genes located within
142 each inversion (Supplementary Tables 1,2,4), made possible by our improved genome
143 assemblies. Third, we determined the location of the proximal breakpoint of *In(16)1*
144 within the gene *FBXW4*, which putatively causes alternative translation start site
145 usage in the *SB* and *Sb* haplotypes. Fourth, we showed that the homologous copies of
146 a “*Jockey-like mobile element*” present at each breakpoint of inversion *In(16)2*
147 provide a likely mechanistic explanation for its origin. Finally, we greatly extended
148 previous work on the effects of chromosome breakpoints on protein-coding gene
149 expression¹¹ by analysing distinct castes and tissue types (Fig. 2). The fire ant
150 supergene is known to influence a vast spectrum of individual- and colony-level trait
151 variation involving all castes (mostly in the adult stages) and comprising diverse
152 social and reproductive contexts^{4,17,18}; thus, analyses of regulatory effects of the *Sb*
153 haplotype in varied biological settings are necessary to begin to link gene function to
154 the complex trait variation observed in this system.

155 Examination of new genome sequences of 19 *Sb* and 60 *SB* males from two distinct
156 South American *S. invicta* populations indicates that a supergene identical in structure
157 and content to the one found in the invasive USA range also mediates polygyny in
158 native populations of this species. Specifically, all native *Sb* males harbour the same
159 three inversions characterizing the *Sb* haplotype in the USA, judging from anomalous
160 read pair (ARP) analyses (Extended Data Fig. 4). Moreover, all of these males were
161 collected from confirmed polygyne colonies (19 colonies from Brazil, Argentina and
162 Uruguay, Supplementary Table 5), consistent with previous work showing a perfect
163 association between polygyny and the presence of allele *Gp-9^b* (which is diagnostic

164 for *Sb*) in native *S. invicta* colonies^{19,20}. In contrast, monogyne colonies (n=34)
 165 produced only *SB* males, and none of these males (nor any of the 26 *SB* males from
 166 polygyne or uncharacterized colonies) harboured any of the three inversions
 167 (Extended Data Fig. 4). Thus, the *Sb* haplotype always carries the same three
 168 inversions, invariably bears allele *Gp-9^b*, and is responsible for regulation of colony
 169 social organisation in native as well as invasive populations of *S. invicta*.

170 Recombination suppression is crucial in the evolution of supergenes because it stably
 171 preserves complementary variants at multiple genes^{8,21}. We therefore calculated the
 172 extent of linkage disequilibrium (LD) across the supergene and over the rest of the
 173 genome for pooled *Sb* and *SB* males of native *S. invicta* to examine the effects of
 174 recombination suppression attributable to the supergene inversions. LD along the
 175 11.4 Mb segment on the distal side of the chromosome 16 centromere was greatly
 176 elevated compared to the rest of the genome (mean $r^2 = 0.35$ vs. 0.03; Mann-Whitney
 177 test, $P < 0.001$; Extended Data Fig. 5a), as was LD along the centromere itself (mean
 178 $r^2 = 0.11$). LD along the larger interval, which corresponds closely to the position of
 179 the three inversions, also is markedly higher among *Sb* than among *SB* males (mean
 180 $r^2 = 0.42$ vs. 0.02; Mann-Whitney test, $P < 0.001$; Extended Data Fig. 5b, c),
 181 suggesting suppression of effective recombination in *Sb* homozygotes as well as in
 182 *SB/Sb* heterozygotes, in contrast to the free recombination assumed to occur among
 183 *SB* homozygotes. Such restriction of effective recombination between *Sb* haplotypes
 184 likely stems from a combination of the recessive lethality of some of these
 185 haplotypes^{22,23} as well as structural constraints or other factors limiting crossing-over
 186 in inversion homokaryotypes²⁴.

187 Because reduced recombination can promote sequence differentiation²⁵, we
 188 quantified both the frequency of fixed differences (d_f) and magnitude of nucleotide
 189 divergence (d_{XY}) between *Sb* and *SB* males. Both of these values were much higher
 190 for the supergene region than for the rest of the social chromosome (d_f : Fig. 3a; d_{XY} :
 191 Extended Data Fig. 6a; Mann-Whitney tests, both $P < 0.01$). The abrupt increase in d_f
 192 and d_{XY} values near position 12.5Mb and decrease near 24.0Mb on chromosome 16
 193 match closely the locations of the distal breakpoint of *In(16)1* and proximal
 194 breakpoint of *In(16)3*, suggesting that the suppression of recombination (manifested

195 as high LD) and consequent high sequence divergence between the *Sb* and *SB*
196 haplotypes are largely attributable to the three inversions.

197 Social polymorphism has been shown to be associated with variation at the *Gp-9*
198 locus in several other fire ant species^{19,20} and was suggested to be regulated by a
199 supergene in the fire ants *Solenopsis richteri* and *S. quinquecupis*²⁶. We sequenced
200 multiple males from each of the five South American species which, together with *S.*
201 *invicta* and *S. quinquecupis*, comprise the so-called “socially polymorphic clade”¹⁹
202 (*S. macdonaghi* [N = 3], *S. megergates* [N = 7], *S. richteri* [N = 56], and the
203 undescribed *S. AdRX* [N = 16] and *S. nr. interrupta* [N = 4]). In each of these five
204 species, we again observed a high level of LD (Extended Data Fig. 7) and elevated
205 sequence divergence (as measured by both d_f and d_{XY} ; Fig. 3 and Extended Data Fig.
206 6) between conspecific *Gp-9^b* and *Gp-9^B* males in the region of chromosome 16
207 corresponding to the *S. invicta* supergene. (We note that the small sample sizes for *Sb*
208 haplotypes in *S. macdonaghi*, *S. megergates*, and *S. nr. interrupta* lead to somewhat
209 inflated values of d_f both within and outside of the supergene because some intra-
210 haplotype polymorphisms are not identified as such owing to sampling error.)
211 Importantly, no *Gp-9^b* (*Sb*) males of any of the six species had ARP reads connecting
212 downstream and upstream regions adjacent to the breakpoints of the three inversions
213 on the *Sb* reference genome (Extended Data Fig. 4a-c) and, similarly, no *Gp-9^B* (*SB*)
214 males had ARP reads connecting analogous regions on the *SB* reference (Extended
215 Data Fig. 4d-f). Together, these data demonstrate that all of the socially polymorphic
216 fire ant species we studied share a homologous inversion-based supergene that is
217 associated with strong suppression of recombination, pronounced sequence
218 divergence between the alternate haplotypes, and polygyne social organization. This
219 confirms previous hypotheses that variation in colony social structure has a common
220 genetic basis in the socially polymorphic clade of South American fire ants⁴.

221 The evolutionary origin of haplotype *Sb* was explored further by conducting a
222 phylogenomic analysis of the socially polymorphic species using SNPs located across
223 all of the genome except the supergene region (N=183 males, Supplementary Table
224 5). The resulting well-resolved and highly supported phylogeny (Fig. 4a) features
225 four major lineages: i) the geographically widespread (native range) and highly
226 invasive *S. invicta*, ii) its undescribed sister species, *S. AdRX*²⁷, iii) the relatively

227 widespread and moderately invasive *S. richteri*, and iv) a cluster of three fairly
228 narrow endemics (*S. nr. interrupta*, *S. megergates*, and *S. macdonaghi*). Phylogenetic
229 trees inferred using only supergene SNPs differed strikingly from the species tree,
230 with the *Sb* haplotypes from all six species invariably forming a strongly supported
231 clade that appears to have originated either just before the radiation producing the
232 known socially polymorphic species (Fig. 4b) (estimated at ~0.51 million years ago;
233 see Extended Data Fig. 8c) or shortly thereafter (Extended Data Fig. 8a,b).
234 Monophyly of the *Sb* haplotype group is consistent with the conclusion reached
235 earlier that the *Gp-9^b* allele assemblage forms a uniquely derived monophyletic group
236 within the *Gp-9* gene tree in fire ants^{3,19,20}.

237 If the *Sb* haplotype lineage originated after the first speciation event, then its presence
238 in all of the species in the socially polymorphic clade would require subsequent
239 hybridization and introgression of *Sb* across species or their stem lineages. As
240 expected, the topology of the *SB* haplotypes is highly congruent with the species
241 relationships; on the other hand, the topology of the *Sb* haplotypes bears less
242 resemblance to the species tree, possibly due to such introgression, selection acting
243 on *Sb* haplotypes²⁸, confinement of *Sb* transmission to only one social form, or
244 occasional intraspecific recombination (“gene flux”) between *Sb* and *SB* haplotypes.

245 The potential occurrence of gene flux is supported by the recent finding of rare *SB/Sb*
246 recombinants in embryo progenies of *S. invicta*¹⁵. Therefore, we undertook formal
247 analyses of the extent to which the three supergene inversions have acted historically
248 as barriers to recombination (i.e., to gene flux between supergene haplotypes and
249 homologous regions of the wild-type conspecific chromosome). ABBA/BABA tests
250 (*D*-statistics) revealed that mutations shared between conspecific *SB* and *Sb*
251 haplotypes significantly exceed the number expected from only recurrent convergent
252 mutation in all six studied species (Fig. 5). Moreover, data from the three best
253 sampled species suggest that gene flux has occurred in both directions (*SB*→*Sb*,
254 *Sb*→*SB*). Direct comparison of shared polymorphic sites (SPS) between the *SB* and
255 *Sb* haplotypes provides additional evidence for historical gene flux, as follows. Given
256 its unique origin, the *Sb* haplotype initially must have been monomorphic. In the
257 absence of gene flux, SPS between *Sb* and *SB* haplotypes can only have arisen
258 through convergent mutations and, therefore, should be rare. Contrary to this

259 expectation, >10% of the polymorphic sites in *Sb* haplotypes also were polymorphic
260 in the *SB* haplotypes, a figure far too high to be attributed solely to recurrent mutation
261 but compatible with occasional historical gene flux between the *SB* and *Sb*
262 haplotypes.

263 Inter-haplotype gene flux is predicted to lead to a negative association between the
264 proportion of SPS and interspecific divergence time when comparing *Sb* and *SB*
265 haplotypes of different species, because more recently diverged species have a longer
266 history of shared ancestry since the origin of *Sb* and, thus, extended opportunities for
267 *Sb-SB* gene flux compared to more distantly related pairs of species that diverged
268 earlier. Consistent with this prediction, SPS were significantly more common within
269 than between each of the two main socially polymorphic clades (*S. invicta-richteri-*
270 *AdRX* and *S. macdonaghi-meergates-nr. interrupta*; Fig. 6a; Mann-Whitney tests,
271 both $P < 0.001$), and there was a strong negative relationship between the proportion
272 of SPS and interspecific nucleotide divergence (d_{XY}) for the three best-sampled
273 species (Fig. 6b, Mantel test, $P < 0.001$). These findings, together with the earlier
274 progeny-study results¹⁵, indicate that recombination between conspecific *Sb* and *SB*
275 haplotypes is not entirely suppressed by the three inversions on *Sb* but has occurred at
276 a low rate following diversification of the socially polymorphic clade.

277 The moderate levels of *Sb* diversity we document (one-third the level of *SB* diversity
278 in *S. invicta*; Fig. 5e) presumably reflect in some measure the effects of such low
279 historical levels of inter-haplotype gene flux. The very different finding by Pracana et
280 al.²⁸ that *Sb* diversity is only a minute fraction (<1%) of *SB* diversity can be explained
281 by the fact that only a few samples from a recently bottlenecked invasive *S. invicta*
282 population were analysed in that study. The presence of such dramatic differences in
283 *Sb* diversity between native and introduced populations predicts corresponding
284 differences in polygyne trait variation and the responsiveness of such traits to
285 selection, an idea supported by earlier findings of strong differences in major features
286 of social organization between Argentine and USA polygyne populations that mirror
287 differences in overall genetic diversity between the two ranges^{29,30}.

288 Large supergenes and sex chromosomes that comprise several inversions are often
289 characterized by “evolutionary strata”, segments of varying sequence divergence that
290 reflect differences in evolutionary age of the inversions^{31,32}. Previous work based on a

291 limited number of *S. invicta* samples from the invasive range showed no evidence for
 292 strata of differentiation along the supergene, leading the authors to propose that a
 293 single event may have led to suppression of recombination over the entire
 294 supergene²⁸. To test this proposal, we examined between-haplotype sequence
 295 differentiation at each of the three inversion regions for the six socially polymorphic
 296 study species as well as for pooled data for subsets of species (clades) using two
 297 different metrics. The rationale for these analyses is the expectation that longer
 298 periods since inversion of a segment are reflected in increased divergence between it
 299 and conspecific wild-type homologs (owing to the reduction in recombination).
 300 Distributions of values for both statistics d_{XY} and d_S among the inversions generally
 301 are as predicted by the hypothesized order of emergence $In(16)1 \rightarrow In(16)2 \rightarrow$
 302 $In(16)3$ for the individual species, a pattern recapitulated in comparisons using
 303 pooled data (Extended Data Fig. 9). The largely congruent single-species patterns are
 304 statistically significant in aggregate (probabilities of no between-inversion differences
 305 in haplotype divergence: $P < 0.05$ for $In(16)1$ vs. $In(16)2$, $P < 0.001$ for $In(16)1$ vs.
 306 $In(16)3$, and $P < 0.005$ for $In(16)2$ vs. $In(16)3$ [Fisher method of combining one-tail
 307 Mann-Whitney test probabilities across species and metrics]). These findings
 308 corroborate Huang et al.'s conclusion¹¹ that $In(16)1$ originated before $In(16)2$, based
 309 on the location/orientation of the doubly inverted fragment, and further indicate that
 310 the centromere-bridging third inversion is the most recent to have appeared.

311 In summary, our study shows that variation in social organisation in the six focal fire
 312 ant species we studied is controlled by a supergene that makes up half of the “social
 313 chromosome.” The *Sb* supergene haplotype evidently evolved via sequential
 314 incorporation of three contiguous inversions. The first inversion to appear caused
 315 minor truncation of the coding sequence of one protein-coding gene, while the second
 316 inversion resulted in broadly manifested increases in expression levels at a second
 317 such gene. The third, most recently acquired, inversion expanded the supergene
 318 boundaries by bridging the centromere and the older inversions. These structural
 319 novelties induced restricted recombination between *Sb* and *SB* haplotypes, which
 320 presumably preserved in alternate sequestered haplotypes the complementary genetic
 321 variants at many co-adapted genes that influence various differences in dispersal and
 322 reproductive strategies between the monogyne and polygyne forms. Important issues
 323 remaining to be resolved are the manner in which such complementary alleles

initially were assembled in the derived *Sb* haplotype³³ and the identities of supergene loci that drove selection to maintain a stable polymorphism in the face of potential Hill-Robertson interference across the linked genes^{31,34,35}. Because the *Sb* haplotype lineage originated near the time of radiation of the socially polymorphic species, it evidently has been maintained through multiple speciation events, leading to a widespread trans-species polymorphism with the *SB* haplotypes. Such polymorphisms, which are rare in nature, reflect the action of persistent balancing selection^{36,37} which, in the case of fire ants, likely is related to the ecological advantages of each social form in different circumstances³⁸ and to the *SB* haplotype opposing the selfish genetic tendencies of *Sb*¹⁵. Finally, our analyses indicate that gene flux (recombination) is not entirely suppressed between the *Sb* and *SB* haplotypes, a result with important implications. Specifically, although crossing-over is expected to be limited in inversion heterozygotes³⁹, gene conversion events may actually be accelerated and yield modest between-haplotype gene flux⁴⁰. Other studies in diverse taxa also have documented sporadic gene flux occurring by double crossovers or gene conversion events between large inverted and wild-type genomic regions analogous to supergene systems⁴¹, even between the X and Y chromosomes in some vertebrates⁴². We therefore suggest that low levels of recombination and/or gene conversion may play an underappreciated role in preventing rapid degeneration of supergenes, by allowing novel variants to infiltrate inversions at a rate insufficient to cause significant decay of LD but sufficient to forestall the effects of Muller's ratchet⁴³, thereby contributing to the persistence of a genetic architecture underlying many complex adaptive polymorphisms.

References:

1. Ross, K. G. Multilocus evolution in fire ants: Effects of selection, gene flow and recombination. *Genetics* **145**, 961–74 (1997).
2. Ross, K. G. & Keller, L. Genetic control of social organization in an ant. *Proc. Natl. Acad. Sci. U. S. A.* **95**, 14232–7 (1998).
3. Krieger, M. J. B. & Ross, K. G. Identification of a major gene regulating complex social behavior. *Science* **295**, 328–332 (2002).
4. Gotzek, D. & Ross, K. G. Genetic regulation of colony social organization in fire ants: an integrative overview. *Q. Rev. Biol.* **82**, 201–226 (2007).
5. Wang, J. *et al.* A Y-like social chromosome causes alternative colony organization in fire ants. *Nature* **493**, 664–668 (2013).
6. Ross, K. & Keller, L. Experimental conversion of colony social organization by manipulation of worker genotype composition in fire ants (*Solenopsis invicta*). *Behav. Ecol. Sociobiol.* **51**, 287–295 (2002).
7. Charlesworth, D. & Charlesworth, B. Theoretical genetics of Batesian mimicry

- 362 II. Evolution of supergenes. *J. Theor. Biol.* **55**, 305–24 (1975).
- 363 8. Schwander, T., Libbrecht, R. & Keller, L. Supergenes and complex
- 364 phenotypes. *Curr. Biol.* **24**, R288–94 (2014).
- 365 9. Thompson, M. J. & Jiggins, C. D. Supergenes and their role in evolution.
- 366 *Heredity* **113**, 1–8 (2014).
- 367 10. Zhang, W., Westerman, E., Nitzany, E., Palmer, S. & Kronforst, M. R. Tracing
- 368 the origin and evolution of supergene mimicry in butterflies. *Nature Commun.*
- 369 **8**, 1269 (2017).
- 370 11. Huang, Y.-C., Dang, V. D., Chang, N.-C. & Wang, J. Multiple large inversions
- 371 and breakpoint rewiring of gene expression in the evolution of the fire ant
- 372 social supergene. *Proc. R. Soc. B Biol. Sci.* **285**, 20180221 (2018).
- 373 12. Ho, M. S., Tsai, P.-I. & Chien, C.-T. F-box proteins: The key to protein
- 374 degradation. *J. Biomed. Sci.* **13**, 181–191 (2006).
- 375 13. Long, M., Betrán, E., Thornton, K. & Wang, W. Chromosome rearrangement
- 376 by ectopic recombination in *Drosophila melanogaster*: Genome structure and
- 377 evolution. *Genetics* **129**, 1085–1098 (1991).
- 378 14. Huang, Y.-C. *et al.* Evolution of long centromeres in fire ants. *BMC Evol. Biol.*
- 379 **16**, 189 (2016).
- 380 15. Ross, K. G. & Shoemaker, D. Unexpected patterns of segregation distortion at
- 381 a selfish supergene in the fire ant *Solenopsis invicta*. *BMC Genetics* **19**, 101
- 382 (2018).
- 383 16. Jaenike, J. Sex Chromosome Meiotic Drive. *Annu. Rev. Ecol. Syst.* **32**, 25–49
- 384 (2001).
- 385 17. Fritz, G. N., Vander Meer, R. K. & Preston, C. A. Selective male mortality in
- 386 the red imported fire ant, *Solenopsis invicta*. *Genetics* **173**, 207–213 (2006).
- 387 18. Lawson, L. P., Vander Meer, R. K. & Shoemaker, D. Male reproductive fitness
- 388 and queen polyandry are linked to variation in the supergene *Gp-9* in the fire
- 389 ant *Solenopsis invicta*. *Proc. R. Soc. B Biol. Sci.* **279**, 3217–3222 (2012).
- 390 19. Gotzek, D., Shoemaker, D. & Ross, K. G. Molecular variation at a candidate
- 391 gene implicated in the regulation of fire ant social behavior. *PLoS One* **2**,
- 392 e1088 (2007).
- 393 20. Krieger, M. J. B. & Ross, K. G. Molecular evolutionary analyses of the
- 394 odorant-binding protein gene *Gp-9* in fire ants and other *Solenopsis* species.
- 395 *Mol. Biol. Evol.* **22**, 2090–2103 (2005).
- 396 21. Charlesworth, D. The status of supergenes in the 21st century: Recombination
- 397 suppression in Batesian mimicry and sex chromosomes and other complex
- 398 adaptations. *Evol. Appl.* **9**, 74–90 (2016).
- 399 22. DeHeer, C. J., Goodisman, M. A. D. & Ross, K. G. Queen dispersal strategies
- 400 in the multiple-queen form of the fire ant *Solenopsis invicta*. *Am. Nat.* **153**,
- 401 660–675 (1999).
- 402 23. Hallar, B. L., Krieger, M. J. B. & Ross, K. G. Potential cause of lethality of an
- 403 allele implicated in social evolution in fire ants. *Genetica* **131**, 69–79 (2007).
- 404 24. Remis, M. I. Chromosome polymorphisms in natural populations of the South
- 405 American grasshopper *Sinipta dalmani*. *Genet. Mol. Biol.* **31**, 42–48 (2008).
- 406 25. Campos, J. L., Charlesworth, B. & Haddrill, P. R. Molecular evolution in
- 407 nonrecombining regions of the *Drosophila melanogaster* genome. *Genome*
- 408 *Biol. Evol.* **4**, 278–288 (2012).
- 409 26. Stolle, E. *et al.* Degenerative expansion of a young supergene. *Mol. Biol. Evol.*
- 410 **36**, 553–561 (2018).
- 411 27. Gotzek, D., Clarke, J. & Shoemaker, D. Mitochondrial genome evolution in

- 412 fire ants (Hymenoptera: Formicidae). *BMC Evol. Biol.* **10**, 300 (2010).
- 413 28. Pracana, R., Priyam, A., Levantis, I., Nichols, R. A. & Wurm, Y. The fire ant
414 social chromosome supergene variant *Sb* shows low diversity but high
415 divergence from *SB*. *Mol. Ecol.* **26**, 2864–2879 (2017).
- 416 29. Ross, K. G. & Shoemaker, D. Estimation of the number of founders of an
417 invasive pest insect population: The fire ant *Solenopsis invicta* in the USA.
418 *Proc. R. Soc. B Biol. Sci.* **275**, 2231–2240 (2008).
- 419 30. Ross, K. G., Vargo, E. L. & Keller, L. Social evolution in a new environment:
420 The case of introduced fire ants. *Proc. Natl. Acad. Sci. U. S. A.* **93**, 3021–3025
421 (1996).
- 422 31. Bachtrog, D. Y-chromosome evolution: Emerging insights into processes of Y-
423 chromosome degeneration. *Nature Rev. Genetics* **14**, 113–124 (2013).
- 424 32. Charlesworth, D., Charlesworth, B. & Marais, G. Steps in the evolution of
425 heteromorphic sex chromosomes. *Heredity* **95**, 118–128 (2005).
- 426 33. Huang, Y.-C. & Wang, J. Did the fire ant supergene evolve selfishly or
427 socially? *Bioessays* **36**, 200–208 (2014).
- 428 34. Comeron, J. M., Williford, A. & Kliman, R. M. The Hill-Robertson effect:
429 Evolutionary consequences of weak selection and linkage in finite populations.
430 *Heredity* **100**, 19–31 (2008).
- 431 35. Kamdem, C., Fouet, C. & White, B. J. Chromosome arm-specific patterns of
432 polymorphism associated with chromosomal inversions in the major African
433 malaria vector, *Anopheles funestus*. *Mol. Ecol.* **26**, 5552–5566 (2017).
- 434 36. Jay, P. *et al.* Supergene evolution triggered by the introgression of a
435 chromosomal inversion. *Curr. Biol.* **28**, 1839–1845. (2018).
- 436 37. Llaurens, V., Whibley, A. & Joron, M. Genetic architecture and balancing
437 selection: the life and death of differentiated variants. *Mol. Ecol.* **26**, 2430–
438 2448 (2017).
- 439 38. Tschinkel, W. R. *The Fire Ants*. (Harvard University Press, 2006).
- 440 39. Stevison, L. S., Hoehn, K. B. & Noor, M. A. F. Effects of inversions on within-
441 and between-species recombination and divergence. *Genome Biol. Evol.* **3**,
442 830–841 (2011).
- 443 40. Crown, K. N., Miller, D. E., Sekelsky, J. & Hawley, R. S. Local inversion
444 heterozygosity alters recombination throughout the genome. *Curr. Biol.* **28**,
445 2984–2990.e3 (2018).
- 446 41. Kelemen, R. K. & Vicoso, B. Complex history and differentiation patterns of
447 the *t*-haplotype, a mouse meiotic driver. *Genetics* **208**, 365–375 (2018).
- 448 42. Grossen, C., Neuenschwander, S. & Perrin, N. The evolution of XY
449 recombination: Sexually antagonistic selection versus deleterious mutation
450 load. *Evolution* **66**, 3155–3166 (2012).
- 451 43. Muller, H. J. The relation of recombination to mutational advance. *Mutat. Res.*
452 *Mol. Mech. Mutagen.* **1**, 2–9 (1964).
- 453 44. Manfredini, F. *et al.* Molecular and social regulation of worker division of
454 labour in fire ants. *Mol. Ecol.* **23**, 660–672 (2014).
- 455 45. Shoemaker, D. & Ascunce, M. S. A new method for distinguishing colony
456 social forms of the fire ant, *Solenopsis invicta*. *J. Insect Sci.* **10**, 73 (2010).
- 457 46. Koren, S. *et al.* Canu: Scalable and accurate long-read assembly via adaptive
458 κ -mer weighting and repeat separation. *Genome Res.* **27**, 722–736 (2017).
- 459 47. Tang, H. *et al.* ALLMAPS: Robust scaffold ordering based on multiple maps.
460 *Genome Biol.* **16**, 3 (2015).
- 461 48. Kielbasa, S. M., Wan, R., Sato, K., Horton, P. & Frith, M. C. Adaptive seeds

462 tame genomic sequence comparison. *Genome Res.* 21, 487–493 (2011).

463 49. Crooks, G. E., Hon, G., Chandonia, J.-M. & Brenner, S. E. WebLogo: A
464 sequence logo generator. *Genome Res.* 14, 1188–1190 (2004).

465 50. Ometto, L., Shoemaker, D., Ross, K. G. & Keller, L. Evolution of gene
466 expression in fire ants: The effects of developmental stage, caste, and species.
467 *Mol. Biol. Evol.* 28, 1381–1392 (2011).

468 51. Valles, S. M. & Porter, S. D. Identification of polygyne and monogyne fire ant
469 colonies (*Solenopsis invicta*) by multiplex PCR of *Gp-9* alleles. *Insectes Soc.*
470 50, 199–200 (2003).

471 52. Picelli, S. et al. Full-length RNA-seq from single cells using Smart-seq2.
472 *Nature Protoc.* 9, 171–181 (2014).

473 53. Dobin, A. et al. STAR: ultrafast universal RNA-seq aligner. *Bioinformatics* 29,
474 15–21 (2013).

475 54. Robinson, M. D., McCarthy, D. J. & Smyth, G. K. edgeR: A Bioconductor
476 package for differential expression analysis of digital gene expression data.
477 *Bioinformatics* 26, 139–140 (2009).

478 55. Van der Auwera, G. A. et al. From fastQ data to high-confidence variant calls:
479 The genome analysis toolkit best practices pipeline. *Curr. Protoc. Bioinf.* 43,
480 11.10.1–11.10.33 (2013).

481 56. McKenna, A. et al. The genome analysis toolkit: A MapReduce framework for
482 analyzing next-generation DNA sequencing data. *Genome Res.* 20, 1297–1303
483 (2010).

484 57. Benjamini, Y. & Hochberg, Y. Controlling the false discovery rate: a practical
485 and powerful approach to multiple testing. *J. Royal Stat. Soc. B* 57, 289–300
486 (1995).

487 58. Chen, K. et al. TIGRA: A targeted iterative graph routing assembler for
488 breakpoint assembly. *Genome Res.* 24, 310–317 (2014).

489 59. Li, H. & Durbin, R. Fast and accurate long-read alignment with Burrows-
490 Wheeler transform. *Bioinformatics* 26, 589–595 (2010).

491 60. Li, H. et al. The sequence alignment/map format and SAMtools.
492 *Bioinformatics* 25, 2078–2079 (2009).

493 61. Garrison, E. & Marth, G. Haplotype-based variant detection from short-read
494 sequencing. *arXiv* (2012).

495 62. Danecek, P. et al. The variant call format and VCFtools. *Bioinformatics* 27,
496 2156–2158 (2011).

497 63. Pitts, J. P., Camacho, G. P., Gotzek, D., Mchugh, J. V. & Ross, K. G. Revision
498 of the Fire Ants of the *Solenopsis saevissima* Species-Group (Hymenoptera:
499 Formicidae). *Proc. Entomol. Soc. Washington* 120, 308–411 (2018).

500 64. Lee, T.-H., Guo, H., Wang, X., Kim, C. & Paterson, A. H. SNPhylo: a pipeline
501 to construct a phylogenetic tree from huge SNP data. *BMC Genomics* 15, 162
502 (2014).

503 65. Stamatakis, A. RAxML version 8: A tool for phylogenetic analysis and post-
504 analysis of large phylogenies. *Bioinformatics* 30, 1312–1313 (2014).

505 66. Reed, E. et al. A guide to genome-wide association analysis and post-analytic
506 interrogation. *Stat. Med.* 34, 3769–3792 (2015).

507 67. Patterson, N. et al. Ancient admixture in human history. *Genetics* 192, 1065–
508 1093 (2012).

509 68. Green, R. E. et al. A draft sequence of the Neandertal genome. *Science* 328,
510 710–722 (2010).

511 69. Moreau, C. S. & Bell, C. D. Testing the museum versus cradle tropical

biological diversity hypothesis: Phylogeny, diversification, and ancestral
 biogeographic range evolution of the ants. *Evolution* 67, 2240–2257 (2013).
 70. Drummond, A. J. & Rambaut, A. BEAST: Bayesian evolutionary analysis by
 sumping trees. *BMC Evol. Biol.* 7, 214 (2007).
 71. Cingolani, P. et al. A program for annotating and predicting the effects of
 single nucleotide polymorphisms, SnpEff. *Fly* 6, 80–92 (2012).
 72. Yang, Z. PAML: A program package for phylogenetic analysis by maximum
 likelihood. *Bioinformatics* 13, 555–556 (1997).
 73. Xu, B. & Yang, Z. PAMLX: a graphical user interface for PAML. *Mol. Biol.*
Evol. 30, 2723–4 (2013).

METHODS

Sample collection. Samples were collected from the native ranges of seven fire ant
 species in South America during collection trips from 1990 to 2015. These were *S.*
invicta, *S. macdonaghi*, *S. megergates*, and *S. richteri*, as well as the undescribed *S.*
AdRX and *S. nr. interrupta*, all members of the “socially polymorphic clade” of South
 American fire ants; *S. saevissima* was sampled as an outgroup species. A total of 169
 specimens from these samples were newly sequenced (Supplementary Table 5). We
 used haploid males exclusively for genome sequencing to directly infer haplotypes.
 We used only a single male from each monogyne colony in order to avoid sequencing
 genetically related individuals and, whenever possible, we sequenced one *Gp-9^b* and
 one *Gp-9^B* male from each polygyne colony. In addition, we used the data from 14
 previously sequenced *S. invicta* males from the invasive (US) range⁵.

Determination of social form. Twelve workers from each colony were genotyped at
 ten highly variable microsatellite loci to verify colony social form by means of
 identifying a single or multiple matriline¹⁹. Additionally, each male specimen was
 typed with a TaqMan allelic discrimination assay at three key codon positions
 considered to be diagnostic for *b*-like alleles of *Gp-9^{44,45}*, with the objective to sample
 as much of the diversity of *Gp-9* alleles and *Sb* haplotypes as possible. All males with
 one or more of the *Gp-9^b* diagnostic codons and possessing the three inversions were
 classified as *Gp-9^b* (*Sb*) individuals, while all those lacking the inversions were
 classified as *Gp-9^B* (*SB*) individuals.

Illumina HiSeq sequencing. Standard Illumina protocols (TruSeq DNA) were used
 to prepare the paired-end libraries. Briefly, genomic DNA was isolated from the

549 whole bodies of single male ants. After fragmentation using a Covaris instrument, the
550 short insert size DNA fragments (target size: 500-550 base pair [bp]) were end
551 repaired and ligated to the Illumina Pair-End Sequencing adapters. Ligated products
552 were PCR-amplified (15 cycles), and each genome library was then sequenced to at
553 least 10X sequencing depth (Supplementary Table 5).

554

555 **Reference genome assembly using PacBio 10kb long reads.** Sequencing data were
556 derived from a single *S. invicta* male pupa with the *SB* haplotype from a Florida, USA
557 polygyne colony, and this served as the basis for the *SB* reference genome assembly
558 (NCBI genome ID *Solenopsis_invicta_M01_SB*). DNA was isolated using the
559 Genomic-tip 20/G extraction Kit (Qiagen) following the manufacturer's instructions.
560 Genomic DNA was sheared to a size range of 15–50 kb using G-tubes (Covaris), and
561 enzymatically repaired and converted into SMRTbell template libraries as
562 recommended by Pacific Biosciences. In brief, hairpin adapters were ligated, after
563 which the remaining damaged DNA fragments and those without adapters at both
564 ends were eliminated by digestion with exonucleases. The resulting SMRTcell
565 templates were size-selected to 15–50 kb by Blue Pippin electrophoresis (Sage
566 Sciences) and sequenced on a PacBio RS II instrument using P6-C4 sequencing
567 chemistry. Data from 40 SMRT cells were collected and 4,061,662 reads
568 (43,553,361,954 bases) were obtained in total. The CANU assembly pipeline version
569 1.4⁴⁶ was used to perform correction of the reads, trim, and assemble. The raw
570 assembly includes 1,447 contigs (N50 size of 956,625 bp). We used JCVI (version
571 0.7.1⁴⁷) to anchor and orient these contigs using three equally-weighted linkage maps
572 constructed from single-queen (*Gp-9^{BB}*) families⁵ with restriction site-associated
573 DNA sequencing (RADseq) SNPs. A total of 64.5% of the contigs (264,123,748 bp)
574 were anchored into 16 linkage groups (chromosomes), with 36.5% of the contigs
575 (144,930,346 bp) remaining unplaced. The total length of contigs located on the
576 social chromosome was 25,360,913 bp, which is 31.4% more than the former gnG
577 assembly version (19,291,722 bp)⁵.

578

579 To identify the inversions that distinguish *Sb* from *SB* haplotypes, we sequenced a
580 single *S. invicta Sb* male pupa from the same colony as above to generate the *Sb*
581 reference genome (NCBI genome ID *Solenopsis_invicta_M02_Sb*), using the
582 identical PacBio RS II protocol. Data from 40 SMRT cells were collected and

3,684,238 reads (46,474,046,294 bp) were obtained in total. The CANU assembly procedure generated 1,372 contigs (N50 size of 1,228,881 bp). We anchored and oriented these contigs using four equally-weighted linkage maps from families headed by single polygyne (*Gp-9^{Bb}*) queens that were previously generated⁵ using RADseq. A total of 86.8% of the contigs (337,734,421 bp) were anchored into 16 linkage groups, with 13.2% of the contigs (51,415,094 bp) remaining unplaced.

Inversions in the supergene. To identify the inversions defining the supergene, a pairwise alignment between the *Sb* and *SB* reference genomes was performed using LAST V531⁴⁸. The last-dotplot script was used to generate a dot plot of the pairwise alignment. To fully characterize the inversion breakpoints, we manually checked the pairwise alignment. The closest nucleotide position separating the alignment into two distant regions along the *SB* haplotype was defined as the breakpoint position. We included 200bp segments upstream and downstream of the breakpoints to calculate sequence similarity between the *Sb* and *SB* haplotypes around the breakpoints.

To test whether the inversions disrupted any protein-coding gene, we downloaded the *S. invicta* Annotation Release 100 from NCBI (https://www.ncbi.nlm.nih.gov/genome/annotation_euk/Solenopsis_invicta/100/) and mapped 14,453 protein-coding genes to the *SB* reference genome. The genome coordinates of these protein-coding genes were compared to the inversion breakpoint coordinates to identify candidate interrupted genes.

To investigate the potential functions of *PGAM2* and *FBXW4*, we compared each protein sequence with its putative orthologs, identified by reciprocal best BLAST among available protein sequences for *Drosophila melanogaster*, *Danio rerio*, *Mus musculus*, and *Homo sapiens* downloaded from NCBI. The catalytic core and typical domains were predicted for *PGAM2* and *FBXW4*, respectively, by InterPro and NCBI. Consensus sequences were produced using WebLogo⁴⁹.

Analysis of expression of genes interrupted by inversion breakpoints. Males and workers were sampled from *Solenopsis invicta* colonies collected in Florida, USA and reared for one month under standard laboratory conditions prior to any experimental manipulations. Males were sampled within one hour after emergence

617 from the pupal stage⁵⁰. Workers, upon reaching the pupal stage, were transferred to
618 polygyne host colonies and maintained for 14 days prior to sampling. Pre-
619 reproductive queens were sampled as they were departing on their mating flights at
620 multiple sites in Georgia, USA. Males and workers were typed with a TaqMan allelic
621 discrimination assay⁴⁵ and queens were typed with a modified multiplex PCR assay⁵¹
622 to determine *Gp-9* haplotypes (males) or genotypes. RNA was extracted from whole
623 bodies of males and from worker brains and gasters (abdomens) using a Trizol
624 protocol. RNA was extracted from queen brains and ovaries using the RNeasy Micro
625 Kit and RNeasy Mini Kit respectively. Sequencing libraries were prepared from male
626 bodies and worker brains using the SMARTer v3 kit for polyA-selected mRNA, from
627 worker gasters using a KAPA stranded RNA-sequencing kit, and from queen brains
628 and ovaries using the SMART-seq2 protocol⁵². All libraries were sequenced using
629 standard Illumina protocols. Sequencing reads are available from the NCBI
630 (PRJNA421367).

631
632 RNA sequencing reads were aligned to the *Solenopsis_invicta_M01_SB* reference
633 genome using STAR's 2-pass approach with default parameters⁵³. Gene counts were
634 then generated based on the Refseq gene models mapped to the
635 *Solenopsis_invicta_M01_SB* reference assembly. Differential expression and gene
636 CPM (counts per million reads) values were computed using edgeR⁵⁴. Additionally,
637 we leveraged fixed, inversion-defining SNPs generated using DNA sequences of *S.*
638 *invicta* males from the native range to compute allele-specific expression at the three
639 inversion breakpoint genes. In heterozygous workers and queens, allele-specific read
640 counts were generated using GATK's ASEReadCounter^{55,56} and allele-specific
641 expression differences were computed using edgeR. Finally, we utilized DEX-seq to
642 quantify differential exon usage between individuals with and without the supergene
643 in each of our sample types. In all analyses, differences were considered significant
644 with an FDR-corrected P-value < 0.05⁵⁷.

645

646 **Inversions in the other socially polymorphic South American fire ant species.**

647 Raw paired-end Illumina sequence reads (PE reads) from 169 males of the six
648 socially polymorphic species were mapped to both the *Sb* and *SB* reference genomes.
649 The raw PE reads that aligned inappropriately to the 800 bp windows around both the
650 proximal and distal inversion breakpoints on the *Sb* or *SB* reference genomes were

651 defined as anomalous read pairs (ARPs). The number of ARPs within each sample
652 was counted separately for inversions *In(16)1*, *In(16)2*, and *In(16)3*. One sample of *S.*
653 *AdRX* and three samples of *S. richteri*, *S. nr. interrupta* and *S. macdonaghi* lacked
654 ARPs directly anchoring the two breakpoints of *In(16)1* and *In(16)3*. Thus, targeted
655 local assembly of breakpoint sequences (TIGRA)⁵⁸ software was used to perform
656 local assembly. The bam files containing raw reads from these samples were
657 extracted as input for TIGRA, and the genome coordinates for the *In(16)3* proximal
658 and distal breakpoints were marked as regions of interest for local assembly. The sets
659 of reads mapped or partially mapped to these regions were assembled into contigs.
660 We further mapped these assembled contigs to the *Sb* and *SB* genomes to confirm that
661 they connected to the *In(16)1* and *In(16)3* breakpoints respectively.

662

663 **Genotype calling and LD analyses.** Illumina paired-end reads from the 190 fire ant
664 male genomes were filtered (minimum quality score 10) and aligned to the reference
665 *SB* genome using bwa 0.7.10⁵⁹. The mapping results were sorted, duplicate marked,
666 and indexed using SAMtools 0.1.19⁶⁰. Because all assembled genomes derived from
667 haploid male specimens, we used the haplotype-based variant detector Freebayes
668 0.9.21⁶¹ to call haplotypes across all individuals with the following parameters:
669 ploidy 1, min-mapping-quality 1, mismatch-base-quality-threshold 10. We detected
670 2,337,243 variants (SNPs) along the social chromosome and 73,406,103 along the
671 remaining 15 chromosomes.

672

673 For the linkage disequilibrium (LD; gametic disequilibrium) analyses, we first used
674 VCFtools 0.1.14⁶² to filter loci (missing data <10%, minor allele frequency >0.2, sites
675 quality value >1000, max alleles =2) in each species. We next used this software to
676 compute r^2 statistics for pairwise LD. The R package gg.ldplot
677 (<https://github.com/timknut/gg.ldplot>) was used to make dot plots to visualize
678 pairwise LD (Extended Data Fig. 5 and Extended Data Fig. 7).

679

680 **Sequence divergence between *Sb* and *SB* haplotypes.** To analyze patterns of
681 differentiation between the *Sb* and *SB* haplotypes in each species, we used VCFtools⁶²
682 to calculate SNP frequencies then employed the script popgenWindows.py
683 (https://github.com/simonhmartin/genomics_general) to compute nucleotide
684 divergence (d_{XY}) using non-overlapping 50 kb sliding windows along chromosome 16.

685 We next used VCFtools⁶² to calculate SNP frequencies and manually computed fixed
686 differences (d_f) between *Sb* and *SB* haplotypes in each species using non-overlapping
687 50 kb sliding windows along chromosome 16. Finally, we used the script
688 popgenWindows.py to compute nucleotide diversity statistics (π) using non-
689 overlapping 50 kb sliding windows along chromosome 16 for *Sb* and *SB* males of the
690 three best-sampled species.

691

692 **Phylogenomic analyses.** We constructed separate phylogenetic trees for the
693 supergene region on chr16 and for the remainder of the genome using all six study
694 species, with *S. saevissima* included as the outgroup in all analyses. This latter
695 species falls outside of the socially polymorphic South American fire ant clade but is
696 placed along with that clade in the *S. saevissima* species-group⁶³; *S. saevissima* lacks
697 the three chr16 inversions characterizing the *Sb* haplotype, thus confirming the *SB*-
698 like chr16 architecture as the ancestral condition for the socially polymorphic clade.
699 For the whole-genome phylogenomic analyses, we constructed a ML tree based on
700 concatenation of 12,237,341 SNPs retained after filtering (supergene region excluded,
701 bi-allelic sites, qual >30). SNPhylo 3.69⁶⁴ was used to construct the whole-genome
702 tree with the following parameter settings: LD threshold 0.1, missing rate 0.1,
703 number of bootstrap replicates 1000. For the supergene analysis, we used RAxML
704 8.1.2⁶⁵ to construct a maximum-likelihood (ML) tree for the 610,247 SNPs with the
705 GTRGAMMA model and 1000 bootstrap replicates. We then used SNPhylo 3.69⁶⁴
706 to construct two additional ML trees that corrected for the strong LD between (non-
707 independence of) supergene SNPs⁶⁶; for these analyses, the LD threshold was set at
708 either 0.5 or 0.8, the missing rate at 0.1, and the number of bootstrap replicates at
709 1000. The best supported supergene phylogeny, with respect to the relationship
710 between *Sb* and *SB* haplotype lineages, was derived from the analysis with the
711 highest level of accommodation of supergene LD (LD threshold=0.8). This tree
712 features 100% bootstrap support between the *Sb* clade (recovered with 100% support
713 in all three trees) and its sister group, in this case a monophyletic *SB* group. The two
714 alternative trees featured 92% or 84% bootstrap support for the relationship between
715 the *Sb* clade and its hypothesized sister-group (in each case, a subset of the *SB*
716 haplotypes).

717

718 **Recombination (gene flux) between the *Sb* and *SB* haplotypes.** The VCF file

719 containing 610,247 SNPs within the supergene region was converted to the
720 EIGENSTRAT format. ADMIXTOOLS 4.1⁶⁷ was used to conduct ABBA/BABA
721 tests⁶⁸ to infer gene flux between conspecific *Sb* and *SB* haplotypes. We used *S.*
722 *saevissima* as the outgroup and examined the numbers of derived alleles shared
723 between three ingroup populations by calculating *D*-statistics. Significance of the *D*-
724 statistics was assessed with a block jackknife procedure using a z score of three
725 standard errors as the threshold⁶⁷.

726

727 As a further means of assessing gene flux, we analyzed patterns of shared
728 polymorphic sites (SPS) between the *Sb* and *SB* haplotypes. We first used VCFtools
729 to calculate frequencies of each variant of the *Sb* and *SB* haplotypes in the focal
730 species or clades. A polymorphic site in both the *Sb* and *SB* haplotypes was classified
731 as a SPS if both haplotypes shared at least two identical bases. The proportion of SPS
732 was defined as the total number of SPS divided by the total number of polymorphic
733 sites within each haplotype. Next, we estimated nucleotide divergence (d_{XY}) between
734 paired socially polymorphic species with all genome-wide SNPs (excluding the
735 supergene region on chr16) using the script popgenWindows.py
736 (https://github.com/simonhmartin/genomics_general). For each of the three species
737 for which we generated five or more *Sb* haplotypes (*S. invicta*, *S. AdRX*, and *S.*
738 *richteri*), we determined the proportion of polymorphic sites in the *Sb* haplotypes that
739 were also polymorphic in the *SB* haplotypes of each of the six species in the socially
740 polymorphic clade (including the focal species). The relationship of the resulting 18
741 SPS values to the nucleotide divergence between paired species (zero in the case of
742 each focal species) was then determined.

743

744 **Times of species divergence and origin of the *Sb* haplotype.** We first estimated the
745 time of origin of the socially polymorphic clade of fire ants and divergence times of
746 the six species using coding sequences of five previously studied nuclear genes (*18S*
747 *rDNA*, *28S rDNA*, *abdominal-A*, *long-wavelength rhodopsin*, and *wingless*)⁶⁹;
748 corresponding sequences from *S. xyloni* (a fire ant not included in the *S. saevissima*
749 species-group⁶³ that was used as the outgroup species) were downloaded from
750 TreeBASE (study accession URL:
751 <http://purl.org/phylo/treebase/phyloids/study/TB2:S11283>; www.treebase.org).
752 Divergence times were estimated using BEAST version 2.4.7⁷⁰, with the GTR+G

753 model of substitution and an uncorrelated log-normal relaxed clock model with a
754 Yule process for the prior on tree topologies. For calibration, a log-normal prior
755 distribution was set with an offset equal to the minimum divergence time between *S.*
756 *xyloni* and *S. invicta* (i.e., 4.5 million years⁶⁹; $\log(\text{mean}) = 1.0$, $\log(\text{SD}) = 1.0$). The
757 MCMC chain was run for 50×10^6 generations and parameters were sampled every
758 1,000 generations. To accelerate convergence, we used the tree obtained by RAxML
759 as a starting tree and prevented the topology from updating by removing the four
760 operators: Wide-exchange, Narrow-exchange, Wilson-Balding, Subtree-slide. We
761 checked the convergence patterns of the MCMC using Tracer and discarded the first
762 10% of chain burn-ins before estimating the posterior distributions using
763 TreeAnnotator.

764

765 **Order of appearance of the three supergene inversions.** Values of d_{XY} between
766 conspecific *Sb* and *SB* haplotypes were estimated for the three inversion regions for
767 each of the six socially polymorphic species. Means and 95% confidence intervals
768 (CIs) were obtained from 1000 bootstrap replicates across homologous non-
769 overlapping 50kb sliding windows ($N=190$, 16, and 21 windows assigned to
770 inversions *In(16)1*, *In(16)2*, and *In(16)3*, respectively, based on the start and end
771 coordinates). The d_{XY} values for each window were averages for all pairs of
772 conspecific *Sb* and *SB* haplotypes. Values of d_{XY} for each inversion region that did not
773 differ significantly between species ($\alpha=0.05$; Kruskal-Wallis [KW] tests followed by
774 Dunn's multiple-comparison tests adjusted using the Benjamini-Hochberg FDR
775 method) were pooled to increase statistical power.

776

777 Values of d_S (number of synonymous substitutions per synonymous site) between
778 conspecific *Sb* and *SB* haplotypes were estimated to complement the d_{XY} analyses.
779 SNPs within the coding regions of *Sb* haplotypes were annotated as synonymous or
780 non-synonymous substitutions by the software SnpEff⁷¹ using the reference *SB*
781 haplotype from *S. invicta*, with the total number of synonymous sites calculated using
782 the software PAML^{72,73}. The genome assembly of the outgroup species *S. saevissima*
783 (not a member of the socially polymorphic South American fire ant clade) was used
784 to aid in assigning ancestral states and thus in designating each SNP in *Sb* haplotypes
785 as a synonymous or non-synonymous substitution. All coding genes in the *Sb*

haplotype with integral open reading frames were assigned to inversion *In(16)1*,
In(16)2, or *In(16)3* ($N=396$, 33, and 16 genes, respectively). Means and 95% CIs for
 d_S were derived from 1000 bootstrap replicates across single homologous genes.
 Values of d_S for each inversion region that did not differ significantly between species
 ($\alpha=0.05$; KW tests followed by Dunn's multiple-comparison tests adjusted using the
 Benjamini-Hochberg FDR method) were pooled to increase statistical power.

Comparisons of d_{XY} and d_S values were used to test for differences among the three
 inversions in their levels of divergence between the homologous *Sb* and *SB*
 haplotypes (i.e., to assess the presence of “evolutionary strata”). Order of appearance
 of the inversions is inferred under the assumption that greater divergence between the
 haplotypes corresponds to greater age of the inversions.

Acknowledgements We thank Keith Harshman for Illumina and Pacbio
 sequencing support, and Roman Arguello, Hugo Darras, Thomas Flatt, Jérôme
 Goudet, Miya Qiaowei Pan, Tanja Schwander, John Wang, and four anonymous
 reviewers for comments on earlier versions of the manuscript. All computations
 were performed at the Vital-IT (<http://www.vital-it.ch>) Center for High-
 Performance Computing (HPC) of the SIB Swiss Institute of Bioinformatics. This
 work was supported by grants from the Swiss NSF to L.K., an ERC Advanced
 Grant to L.K., U.S. NSF grants to K.R. and D.S. (1354479) and K.R. and B.H.
 (1755130), and U.S. Federal Hatch funds to K.R. and B.H.

Author contributions D.G., K.R., D.S. and L.K. designed the experiments. K.R.,
 D.S. and D.G. performed sample collection, DNA extraction, and genotyping. Z.Y.
 performed Pacbio sequence data collection and genome assembly and analyzed the
 population genomic data. Z.Y., P.D., N.S., and L.K. conducted phylogenomic
 analyses. S.V.A, Z. Y., O.R.-G. and B.H. performed RNA-seq analyses. Q.H.
 conducted analyses of the structure of the genes interrupted by the inversions. S.M.
 performed population genetic simulations. Z.Y., K.R. and L.K. wrote the
 manuscript with the help of all authors.

Data availability The genome assembly, gene models, and sequence reads are
 available at the NCBI under the BioProject PRJNA421367.

Competing interests The authors declare no competing financial interests.

822 **Fig. 1| The three inversions that distinguish the *Sb* and *SB* haplotypes on the fire ant**
823 **social chromosome (chr16). a:** Dot plot of the sequence alignment between chr16 of *Sb* and
824 *SB* males of *S. invicta* (pairwise alignment of NCBI genome ID
825 *Solenopsis_invicta_M01_SB* with *Solenopsis_invicta_M02_Sb*). Grey dots indicate the
826 forward strand alignment and dots of other colors the reverse strand alignment; the three
827 major non-grey lines correspond to the three inversions. The centromere region is defined by
828 the presence of centromeric satellite sequences. **b:** Evolution of the *Sb* haplotype from an *SB*-
829 like haplotype by acquisition of three inversions [*In(16)1*, *In(16)2*, and *In(16)3*], arranged in
830 order of their inferred evolutionary appearance (Extended Data Fig. 9). White and black
831 arrows indicate locations of proximal and distal breakpoints, respectively, of each inversion
832 (with associated genomic coordinates). Note the short overlap (586nt) between the proximal
833 breakpoint of inversion *In(16)1* and distal breakpoint of *In(16)2*, indicating that this fragment
834 was inverted twice. Coding genes disrupted by the inversions are shown in grey boxes
835 (***FBXW4***: *F-box/WD repeat-containing protein 4-like* gene; ***PGAM2 5' UTR***:
836 *Phosphoglycerate mutase 2* gene 5' UTR; ***unchar. 5' UTR***: uncharacterized gene 5' UTR).
837 Structures are not all drawn to scale.

839

840 **Fig. 2| Expression of three protein-coding genes interrupted by supergene inversion**

841 **breakpoints in *S. invicta*.** Gene expression levels from RNA-seq data are plotted in counts
842 per million (CPM) mapped reads for samples that differ in their social chromosome genotype,
843 including whole bodies of *Sb* and *SB* males (N = 4/haplotype), brains and ovaries of *Sb/Sb*,
844 *SB/Sb*, and *SB/SB* pre-reproductive queens (N = 7-8/genotype), and brains and gasters
845 (abdomens) of *SB/Sb* and *SB/SB* workers (N = 6-8/genotype). The box ranges from the first
846 (Q1) to the third quartile (Q3) of the distribution and represents the interquartile range (IQR).
847 A line across the box indicates the median. The whiskers are lines extending from Q1 and Q3
848 to end points that are defined as the most extreme data points within $Q1 - 1.5 \times IQR$ and $Q3$
849 $+ 1.5 \times IQR$, respectively. Each expression value is represented by a hollow circle.
850 Significance designations refer to P-values following FDR correction as described in the
851 Methods.

852

853 **Fig. 3| Fixed difference (d_f) values across the social chromosome between conspecific *Sb***
854 **and *SB* males of six socially polymorphic fire ant species estimated using 50kb non-**
855 **overlapping sliding windows.** The boundaries of the differently coloured intervals
856 correspond to the breakpoints of the three inversions, with the inversions depicted by thick
857 horizontal coloured lines. The x-axes represent physical position along chr16, with the
858 location of gene *Gp-9* indicated. In each of the six species, d_f was significantly higher
859 between the *Sb* and *SB* haplotypes than between the sequences of *Sb* and *SB* males across the
860 rest of the social chromosome (Mann-Whitney tests, all $P < 0.001$).

861

862 **Fig. 4| Phylogenies of South American fire ant species in the “socially polymorphic**
863 **clade” and of the supergene region in these species.** Maximum-Likelihood (ML)
864 phylogenetic trees feature triangular terminals that represent collapsed nodes of related
865 sequences (100% bootstrap support); height is proportional to the number of sequenced males
866 (shown in parentheses after species name) comprising each collapsed node. Bootstrap support
867 values are shown at relevant nodes. Trees were rooted using sequences from the outgroup
868 species *S. saevissima*, which lacks the chr16 inversions. The red scale bars are substitutions
869 per site. **a:** Species tree of the six species based on 12,237,341 genome-wide SNPs, excluding
870 those in the supergene. Crosshatching indicates the presence of both monogyny and polygyny
871 and of both the *Sb* and *SB* haplotypes in a species. **b:** Tree of the *Sb* and *SB* haplotypes of
872 chr16 in the six species based on 610,247 SNPs and that accounts for LD, using a pruning
873 threshold of 0.8. The dark and light blue colors represent sequences recovered from *Sb* and
874 *SB* males, respectively. The vertical dotted lines highlight the positions of two major
875 haplotype groups in the phylogeny (the *SB* and *Sb* clades).

876

877 **Fig. 5| Results of ABBA/BABA tests (D statistics) for recombination (gene flux) between**
878 **conspecific *Sb* and *SB* haplotypes and estimates of nucleotide diversity (π).**

879 ABBA/BABA tests were performed for each of the six socially polymorphic *Solenopsis* study
880 species **a:** to detect gene flux from *SB* into conspecific *Sb* haplotypes by comparing focal *SB*
881 males to conspecific and heterospecific *Sb* males and **b:** to detect gene flux in the opposite
882 direction by comparing focal *Sb* males to conspecific and heterospecific *SB* males. **c:** Gene
883 flux from *SB* into conspecific *Sb* haplotypes; for each of the six species, D statistics from the
884 ABBA/BABA tests were computed by using *Sb* haplotypes from each of the three most
885 distantly related species for the heterospecific comparisons (i.e., for each species there are
886 three points of the same color indicating the values of these three estimates). Error bars
887 indicate ± 3 standard errors estimated with a weighted-block jackknife approach using 50 kb
888 blocks of the complete supergene region; non-overlap with zero signifies a statistically
889 significant D -value (evidence for gene flux). **d:** Gene flux from *Sb* into conspecific *SB*
890 haplotypes was measured as in **(c)** but with *SB* males used as referents to estimate gene flow
891 in the opposite direction. **e:** Nucleotide diversity (π) within the supergene region for *Sb* and
892 *SB* males of the three best-sampled species (native ranges); error bars indicate the 95% CIs
893 about the means derived from resampling of 228 non-overlapping 50kb windows. Nucleotide
894 diversity was significantly lower in *Sb* than *SB* males in each of the species (t -tests, all
895 $P < 0.001$). The relatively modest difference in diversity between *Sb* and *SB* in *S. invicta* (as
896 well as the other two species), stands in stark contrast to the extreme reduction in *Sb* diversity
897 relative to *SB* diversity in invasive *S. invicta* portrayed in Pracana et al.²⁸.

898
899
900
901
902
903
904
905
906
907
908
909
910
911
912
913
914
915
916

Fig. 6| Proportions of shared polymorphic sites (SPS) between *Sb* and *SB* haplotypes of different species. a: Left panel–SPS between *Sb* haplotypes from the *S. invicta-richteri-AdRX* clade and *SB* haplotypes from the same clade (red bar) or from the *S. macdonaghi-megergates-nr. interrupta* clade (blue bar); right panel–SPS between *Sb* haplotypes from the *S. macdonaghi-megergates-nr. interrupta* clade and *SB* haplotypes from the same clade (red bar) or from the *S. invicta-richteri-AdRX* clade (blue bar). Error bars represent 95% confidence intervals (CIs) from 1,000 resampling iterations. **b:** SPS between *Sb* haplotypes from the three best-sampled species (*S. invicta*, *S. richteri*, and *S. AdRX*) and *SB* haplotypes from all six socially polymorphic species studied plotted against interspecific nucleotide divergence (d_{XY}). The green zone defines the 95% confidence level interval for predictions from a negative linear regression model ($r=-0.82$). Historical gene flux is predicted to lead to a negative relationship between the proportion of SPS and divergence time when comparing *Sb* and *SB* haplotypes of different species because more closely related (recently diverged) species have a longer history of shared ancestry since *Sb* originated and, thus, greater opportunities for gene flux between *SB* and *Sb*, than more distantly related species. This prediction is supported by the greater within-clade than between-clade SPS as well as the negative correlation between proportion of SPS and d_{XY} .

917

918 **Extended data Fig. 1| Dot plot of the alignment between chromosomes 1-15 of *Sb* and**
919 ***SB* males of *S. invicta* from the invasive (USA) range. The red line indicates the forward**
920 strand alignment.

921
922 **Extended data Fig. 2| Sequence features for the breakpoints of the three *Sb* supergene**
923 **inversions, *In(16)1* [chr16:14,549,064-24,031,576], *In(16)2* [chr16: 13,705,210-**
924 **24,030,990], and *In(16)3* [chr16: 12,612,565-13,683,100]. a:** The red and blue blocks
925 represent the 200nt segments adjacent to the *In(16)1* proximal breakpoint (red arrow), and the
926 magenta and gold blocks represent the 200nt segments adjacent to the distal breakpoint
927 (black arrow) of this inversion. The blue and magenta blocks, and the segment between them,
928 are inverted between *SB* and *Sb*, as indicated by the gray arrow. The *Sb* haplotype has a 9nt
929 insertion at the proximal breakpoint and a 27,953nt insertion at the distal breakpoint (black
930 blocks). Percentages are the sequence similarity (disregarding deletions) between *SB* and *Sb*
931 for the 200nt segments immediately upstream and downstream of the breakpoints. **b:** The
932 *In(16)1* proximal breakpoint (red arrow) on the *SB* haplotype is located in exon 1 of the “*F-*
933 *box/WD repeat-containing protein 4-like*” gene (NCBI Gene symbol: LOC105199310; green
934 blocks depict exons; pale green represents the UTRs and dark green the coding sequence
935 [CDS] regions). The red and blue lines under exon 1 indicate the segments that are upstream
936 or downstream of the proximal breakpoint. **c:** The *In(16)1* distal breakpoint (black arrow) on
937 the *SB* haplotype is located in the 5’ UTR of the “*Phosphoglycerate mutase 2*” gene (NCBI
938 Gene symbol: LOC105193833; green blocks depict exons; pale green represents the UTRs
939 and dark green the CDS regions). The red and blue lines under exon 1 indicate the segments
940 that are upstream or downstream of the distal breakpoint. **d:** The red and blue blocks
941 represent the 200nt segments adjacent to the *In(16)2* proximal breakpoint (red arrow), and the
942 magenta and gold blocks the 200nt segments adjacent to the distal breakpoint (black arrow)
943 of this inversion. The red block contains the 3’ end of a Jockey-like mobile element. The *Sb*
944 haplotype has a 14nt insertion (black block) at the proximal breakpoint as well as a second
945 Jockey-like mobile element gene (pink block) and a 10,310nt insertion (black block) just
946 upstream of the distal breakpoint. **e:** The *In(16)2* proximal breakpoint (red arrow) in the *SB*
947 haplotype is located in the single exon (dark green) of a Jockey-like mobile element. **f:** The
948 *In(16)2* distal breakpoint (black arrow) in the *SB* haplotype is located in the 5’ UTR of the
949 uncharacterized gene “LOC105193832” (containing 3 exons depicted as green blocks; pale
950 green represents the UTR and dark green the CDS region). **g:** The red and blue blocks
951 represent the 200nt segments adjacent to the *In(16)3* proximal breakpoint (red arrow), and the
952 magenta and gold blocks the 200nt segments adjacent to the distal breakpoint (black arrow)
953 of this inversion. The *SB* haplotype has a 334nt insertion at the proximal breakpoint and a
954 3,100nt insertion at the distal breakpoint (black blocks); both are absent in the *Sb* haplotype,
955 which instead has a 62,682nt insertion at the proximal breakpoint and a 142nt insertion at the
956 distal breakpoint (black blocks). **h:** The *In(16)3* proximal breakpoint (red arrow) in the *SB*
957 haplotype is located just upstream of a region containing 24 dinucleotide (AT) repeats. **i:** The

958 *In(16)3* distal breakpoint (black arrow) in the *SB* haplotype is located within a region
959 containing 21 dinucleotide (AT) repeats.

960
961 **Extended data Fig. 3| Functional features of the two protein-coding genes interrupted**
962 **by the inversion *In(16)I* breakpoints. a:** The *S. invicta* *Phosphoglycerate mutase 2*
963 (*PGAM2*) protein sequence shows a very high level of similarity with putative orthologs in
964 *Drosophila melanogaster* (fruit fly), *Danio rerio* (zebrafish), *Mus musculus* (mouse), and
965 *Homo sapiens*. Virtually all described functional sites are conserved across the five species:
966 the catalytic core is strictly conserved and all but one amino acid of the substrate binding
967 sites are also conserved. This high level of amino acid sequence conservation suggests
968 conservation of the function of *PGAM2* among putative orthologs. **b:** The *S. invicta* *FBXW4*
969 protein contains the typical domains of F-box protein ubiquitin ligase complexes (F-box and
970 WD40 repeats from InterPro and NCBI predictions) and is therefore also likely to be
971 involved in ubiquitination and proteasome degradation. In the alignment, identical sites are
972 shown with black bars, 75% similar with dark grey, 50% with light grey, and 25% with white.
973 **c:** Disruption of *PGAM* in *D. melanogaster*, the ortholog of *PGAM2* in *S. invicta*, is not lethal.
974 Paralogous of *S. invicta* *FBXW4* in *D. melanogaster* have a wide range of substrates and their
975 disruption can be lethal.

976

977 **Extended data Fig. 4| The box plot of the numbers of anomalous read pairs (ARPs)**
978 **connecting the downstream and upstream regions (400nt) adjacent to the breakpoints of**
979 **the three supergene inversions [*In(16)1*, *In(16)2*, *In(16)3*] for *Sb* and *SB* males of six**
980 **socially polymorphic fire ant species.** The box ranges from the first (Q1) to the third
981 quartile (Q3) of the distribution and represents the interquartile range (IQR). A line across the
982 box indicates the median. The whiskers are lines extending from Q1 and Q3 to end points
983 that are defined as the most extreme data points within $Q1 - 1.5 \times IQR$ and $Q3 + 1.5 \times IQR$,
984 respectively. Each outlier outside the whiskers is represented by a solid dot. **a-c:** ARPs
985 connecting proximal and distal inversion breakpoints when samples are mapped to the *Sb*
986 reference genome. **d-f:** ARPs connecting proximal and distal inversion breakpoints when
987 samples are mapped to the *SB* reference genome. There are four *Gp-9^b* individuals with zero
988 values when samples are mapped on the *SB* reference genome (one *S. AdRX* for inversion
989 *In(16)1*); one *S. richteri*, one *S. nr. interrupta*, and one *S. macdonaghi* for inversion *In(16)3*).
990 However, the targeted local assembly of the breakpoint sequences yielded contigs that bridge
991 these breakpoints in *Sb* males of all these four individuals.

992
993 **Extended Data Fig. 5| Linkage disequilibrium (r^2 ; =gametic disequilibrium for haploid**
994 **males) in native *S. invicta* estimated using SNPs across the social chromosome (chr16).**
995 **a:** LD dot plot for pooled *SB* (N=60) and *Sb* (N=19) males. **b:** LD plot for *Sb* males. **c:** LD
996 plot for *SB* males. The colored bar under each plot represents the physical map of the
997 chromosome, with the red segment indicating the region where recombination is suppressed
998 between the *Sb* and *SB* haplotypes in invasive (USA) *S. invicta*. SNPs are ordered according
999 to physical position on the chromosome. The blue and red dashed lines link SNPs on the LD
1000 plot to their position on the physical map. The centromere occupies the approximate region
1001 7.5-11Mb.

1002
1003 **Extended Data Fig. 6| Nucleotide divergence (d_{XY}) values between sequences from**
1004 **conspecific *Sb* and *SB* males of the six socially polymorphic fire ant species estimated**
1005 **using 50kb non-overlapping sliding windows across the social chromosome. The**
1006 boundaries of the differently shaded intervals correspond to the breakpoints of the three
1007 inversions, with the inversions depicted by thick horizontal colored lines. The x-axes
1008 represent physical position along chromosome 16, with the location of gene *Gp-9* indicated.
1009 For each of the six species, d_{XY} values between *Sb* and *SB* males were significantly higher for
1010 the region corresponding to the inversions than for the rest of the social chromosome (Mann-
1011 Whitney tests, all $P < 0.01$). The region of elevated d_{XY} proximal to the inversions (at ca. 8-10
1012 Mb) appears to experience reduced recombination in *S. invicta* based on progeny studies¹⁵;
1013 this area may correspond at least partly to the centomeric region or some other, unknown
1014 feature may be responsible for the reduced recombination and elevated d_{XY} there.
1015

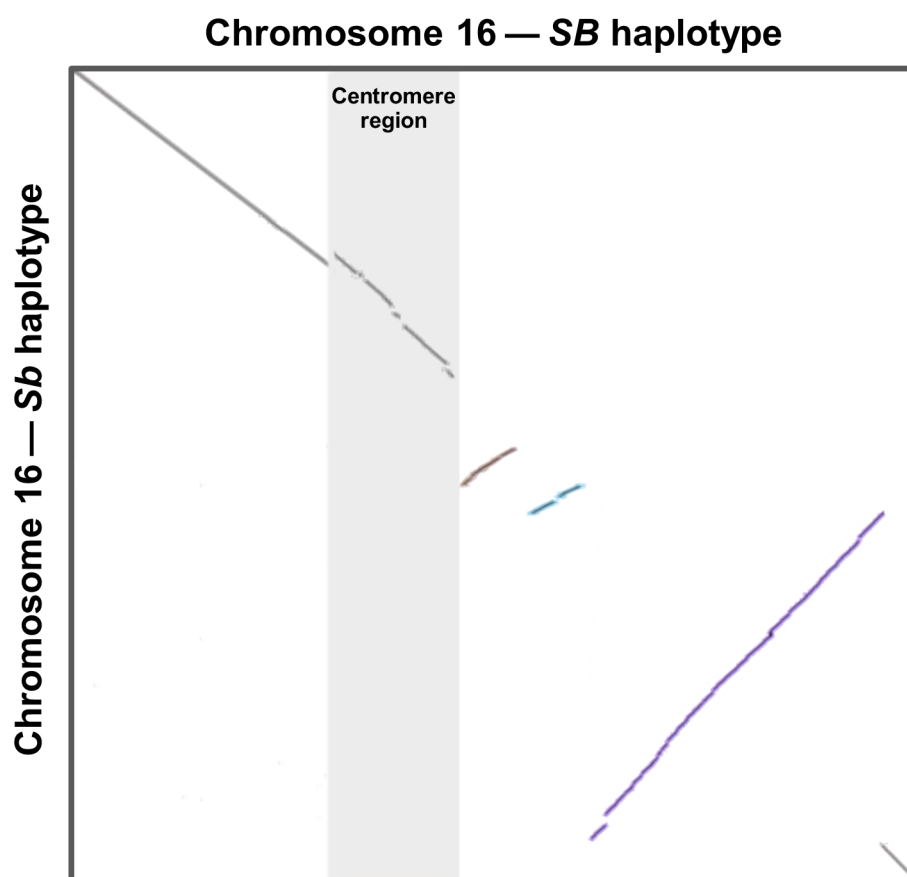
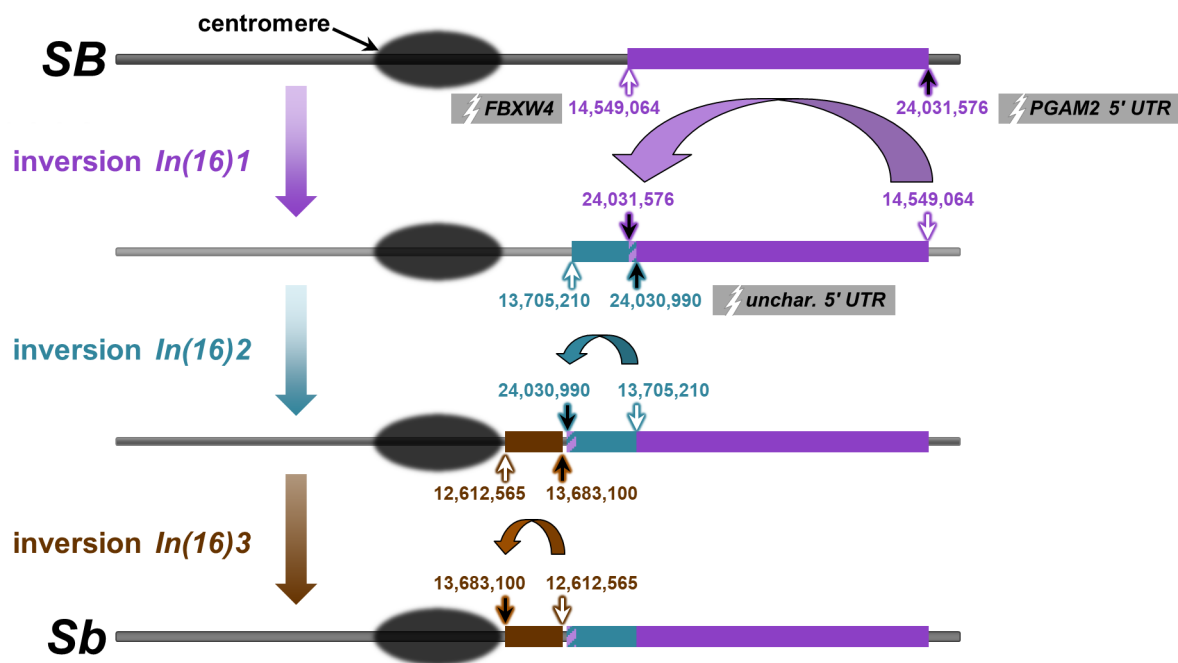
1016
1017 **Extended data Fig. 7| Linkage disequilibrium (r^2 ; =gametic disequilibrium) for pooled**
1018 **conspecific *Sb* and *SB* males of five native populations of socially polymorphic fire ants**
1019 **estimated using SNPs across the social chromosome. a:** LD dot plot for pooled *Sb* (N=30)
1020 and *SB* (N=26) *S. richteri* males. **b:** LD plot for *Sb* (N=5) and *SB* (N=11) *S. AdRX* males. **c:**
1021 LD plot for *Sb* (N=2) and *SB* (N=2) *S. nr. interrupta* males. **d:** LD plot for *Sb* (N=1) and *SB*
1022 (N=2) *S. megergates* males. **e:** LD plot for *Sb* (N=1) and *SB* (N=2) *S. macdonaghi* males.
1023 Mean LD estimates for exclusively *Sb* haplotypes are $r^2 = 0.41, 0.36, 0.85, 0.87,$ and 0.80 for
1024 *S. richteri*, *S. AdRX*, *S. megergates*, *S. nr. interrupta*, and *S. macdonaghi*, respectively. See
1025 Extended Data **Fig. 5** caption for additional information.

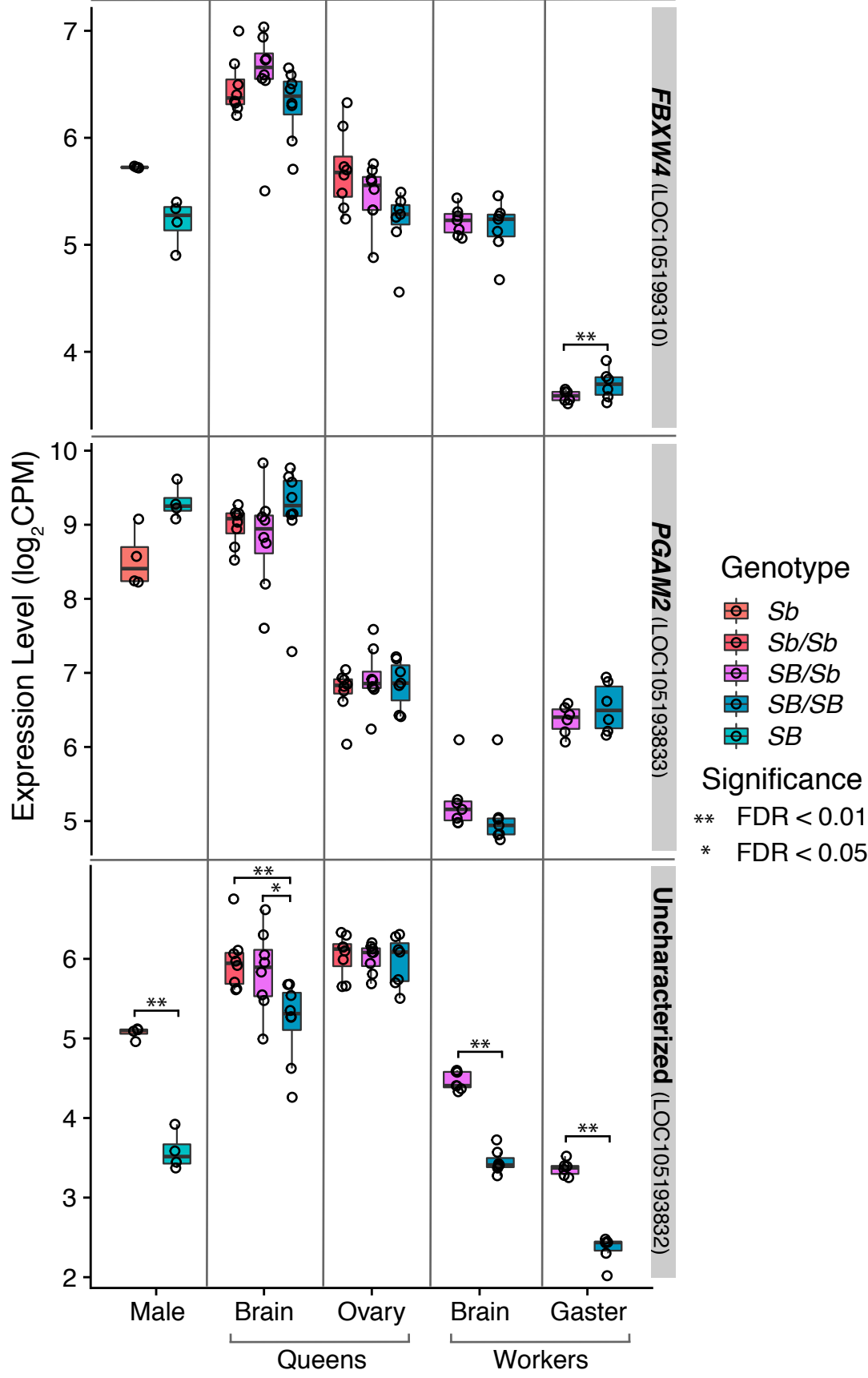
1026
1027 **Extended data Fig. 8| Phylogenetic trees for the supergene region of the social**
1028 **chromosome and for the fire ant species included in this study. a:** Alternative maximum-
1029 likelihood (ML) tree for the supergene region that disregards the LD (non-independence) of
1030 the 30,921 included SNPs. **b:** Alternative ML tree for the supergene region that accounts for
1031 LD, using a pruning threshold of 0.5. Trees in **(a)** and **(b)** were rooted with the outgroup
1032 species *S. saevissima*, which lacks the three chr16 inversions. The red scale bars are
1033 substitutions per site. **c:** Bayesian-inference tree with divergence time estimates for the study
1034 species based on sequences of five nuclear genes. The analysis incorporated the uncorrelated
1035 molecular clock method (BEAST), with the age of the basal divergence calibrated using data
1036 from a previous study (see Methods). The tree was rooted with the outgroup species *S. xyloni*.
1037 The number at each node represents the mean estimate of divergence time (in Myr), with the
1038 green bars representing the 95% confidence intervals (CIs) about the estimates; divergence
1039 time for the two major lineages of the socially polymorphic clade is highlighted with yellow
1040 background. Note that the topology of this tree is fully congruent with that of the ML species
1041 tree based on 12,237,341 non-supergene SNPs (Fig. 4).
1042

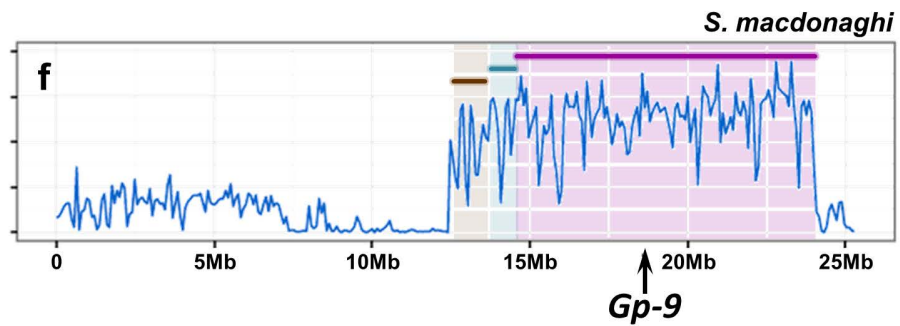
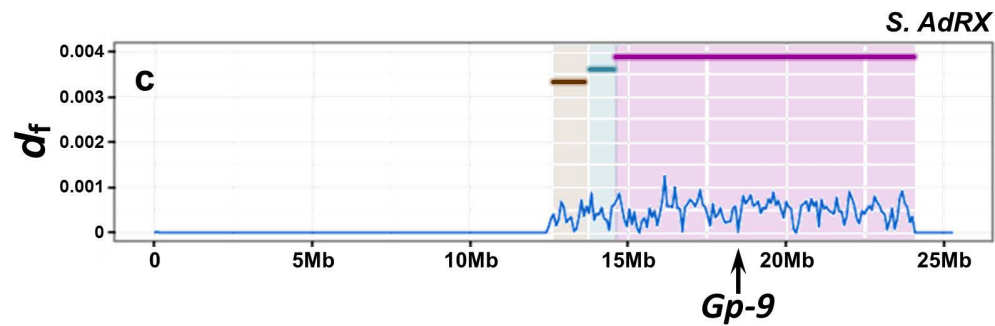
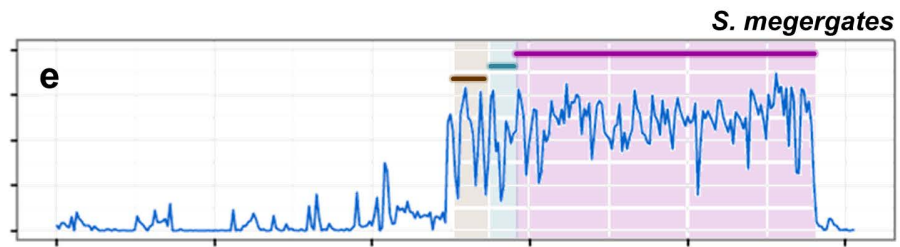
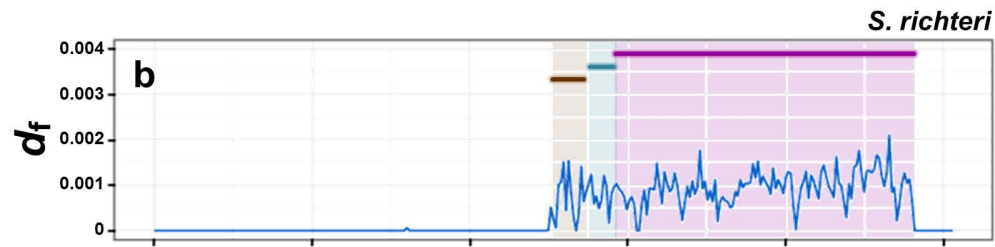
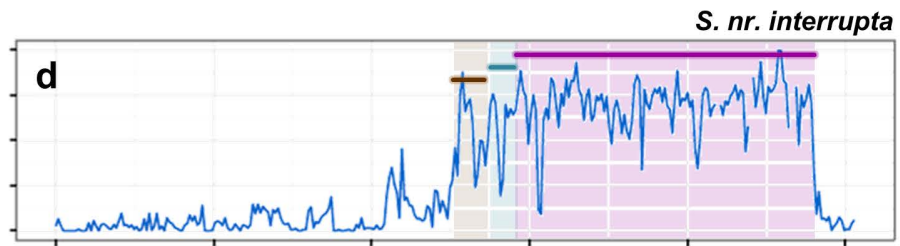
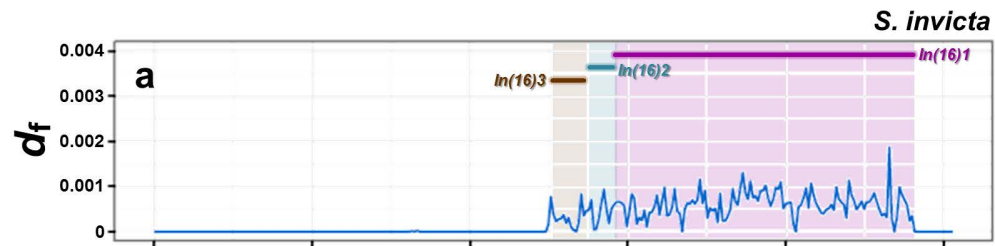
1043

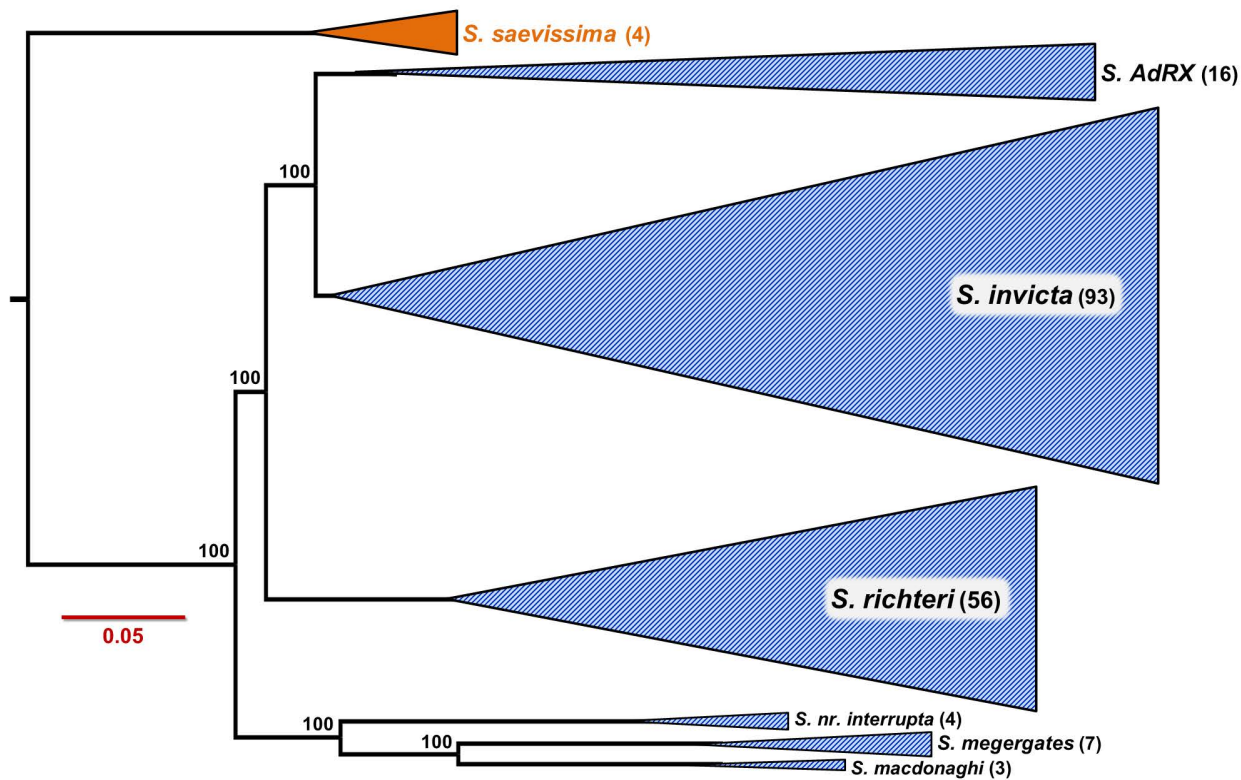
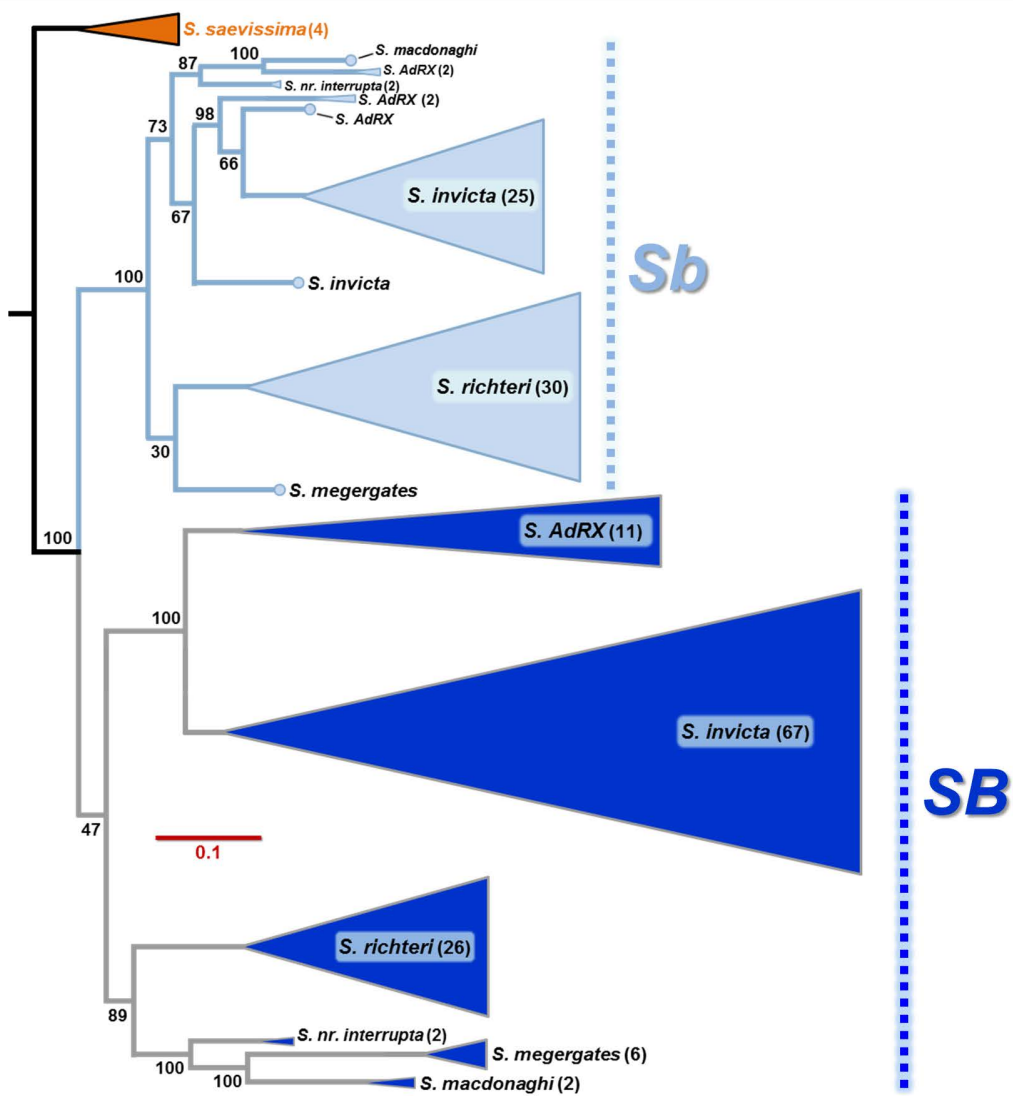
1044 **Extended Data Fig. 9| Evidence from d_{XY} and d_S estimates that the three inversions**
1045 **comprising the *Sb* haplotype emerged in the order *In(16)1*→*In(16)2*→*In(16)3*.**

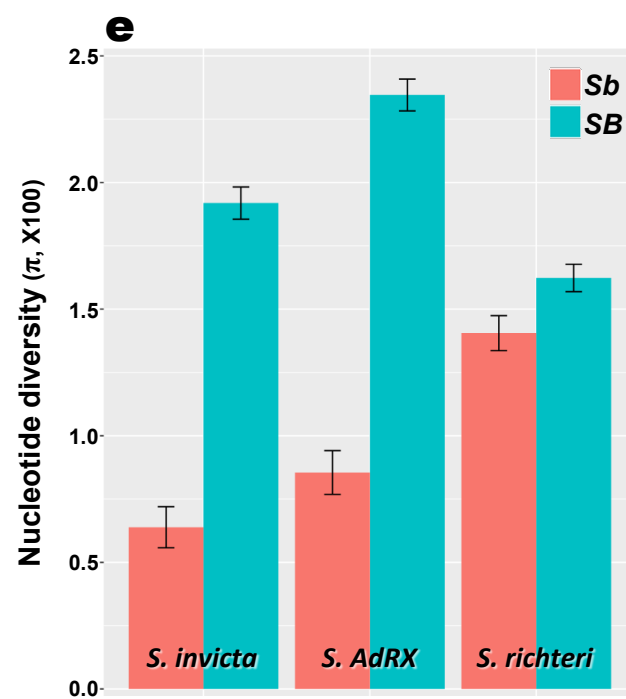
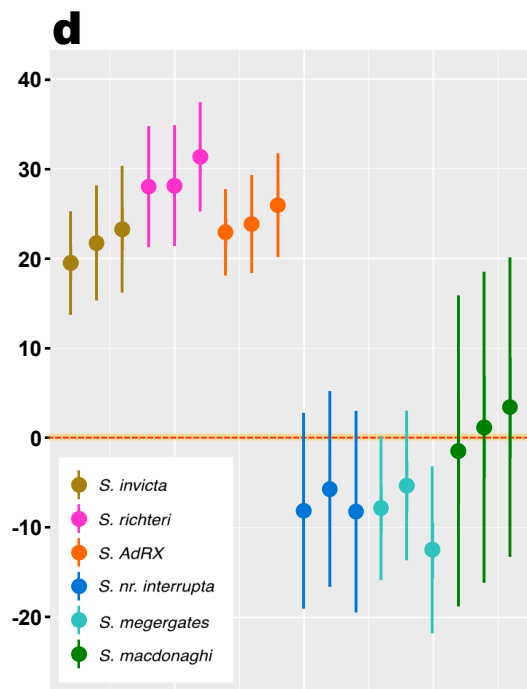
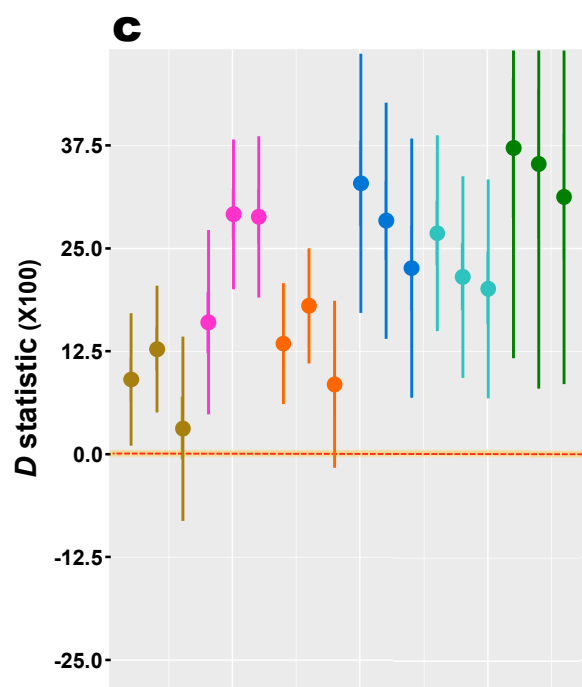
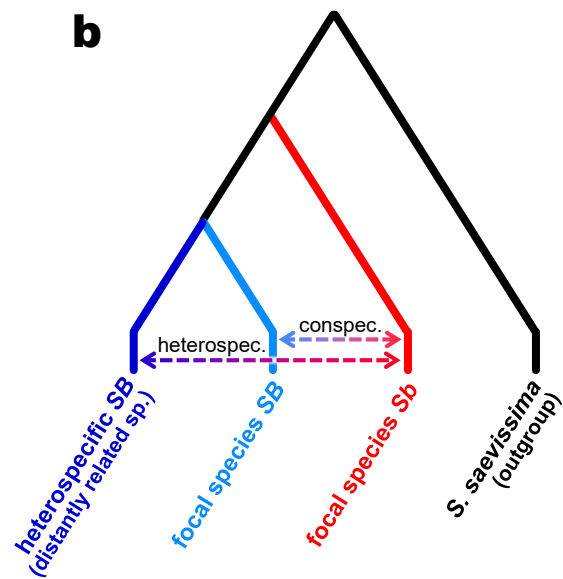
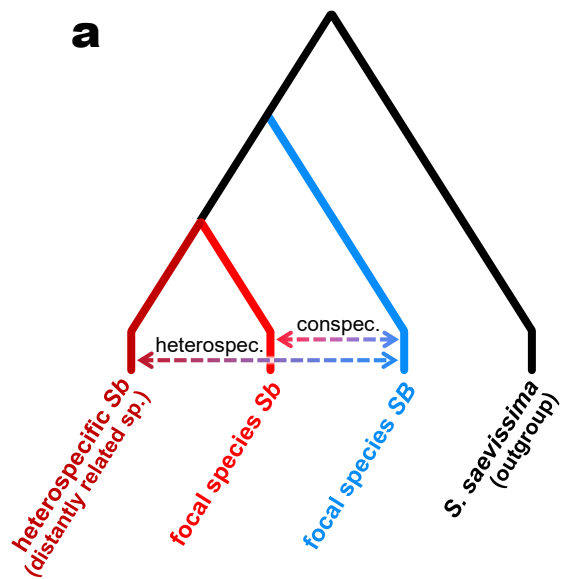
1046 **a:** Values of d_{XY} between conspecific *Sb* and *SB* haplotypes for the three inversions in each of
1047 the six socially polymorphic fire ant species studied (left panel) and for groups of species for
1048 which data were pooled (right panel) (means and 95% CIs from 1000 bootstrap replicates).
1049 Values for subsets of species were pooled if they did not differ significantly (see Methods).
1050 Note that d_{XY} values for *S. macdonaghi*, *S. megerates*, and *S. nr. interrupta* may not be
1051 highly accurate because of the small sample sizes for *Sb* in these species. **b:** Values of d_S
1052 between conspecific *Sb* and *SB* haplotypes for the three inversions in each of the six socially
1053 polymorphic fire ant species studied (left panel) and for groups of species for which data
1054 were pooled (right panel) (means and 95% CIs from 1000 bootstrap replicates). Values for
1055 subsets of species were pooled if they did not differ significantly (see Methods). Note that d_S
1056 values for *S. macdonaghi*, *S. megerates*, and *S. nr. interrupta* may be inflated because the
1057 small sample sizes of *Sb* for these species mean that some intra-haplotype polymorphic
1058 synonymous changes are interpreted to be fixed synonymous differences.

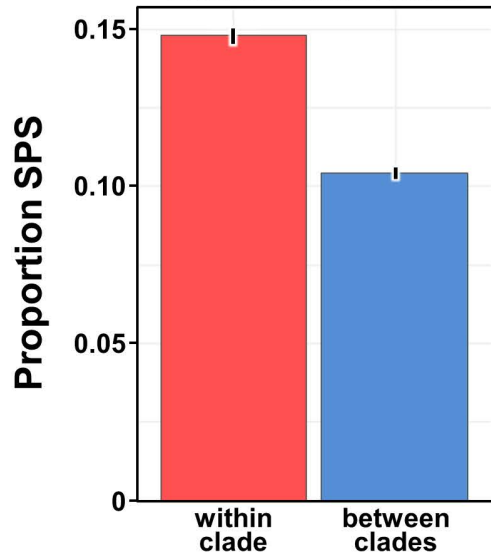
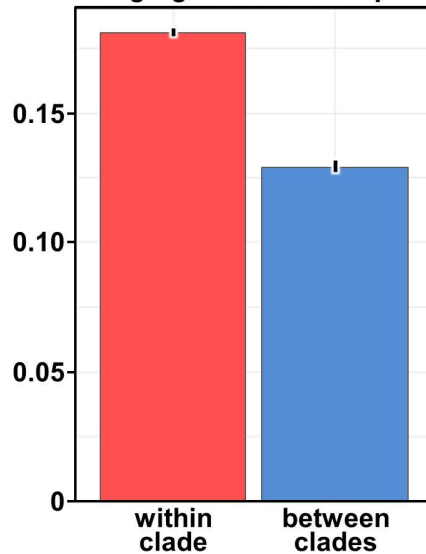
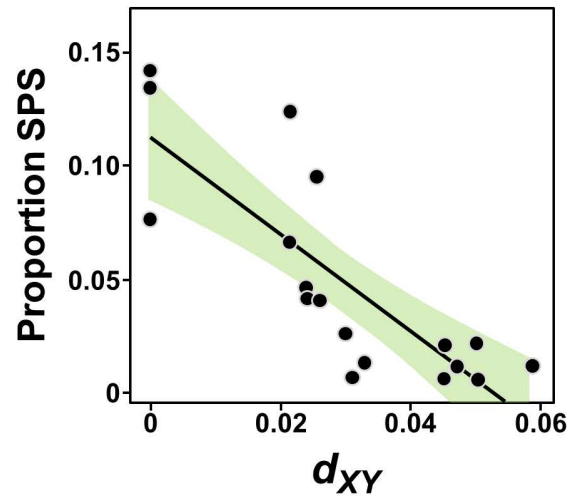
a**b**





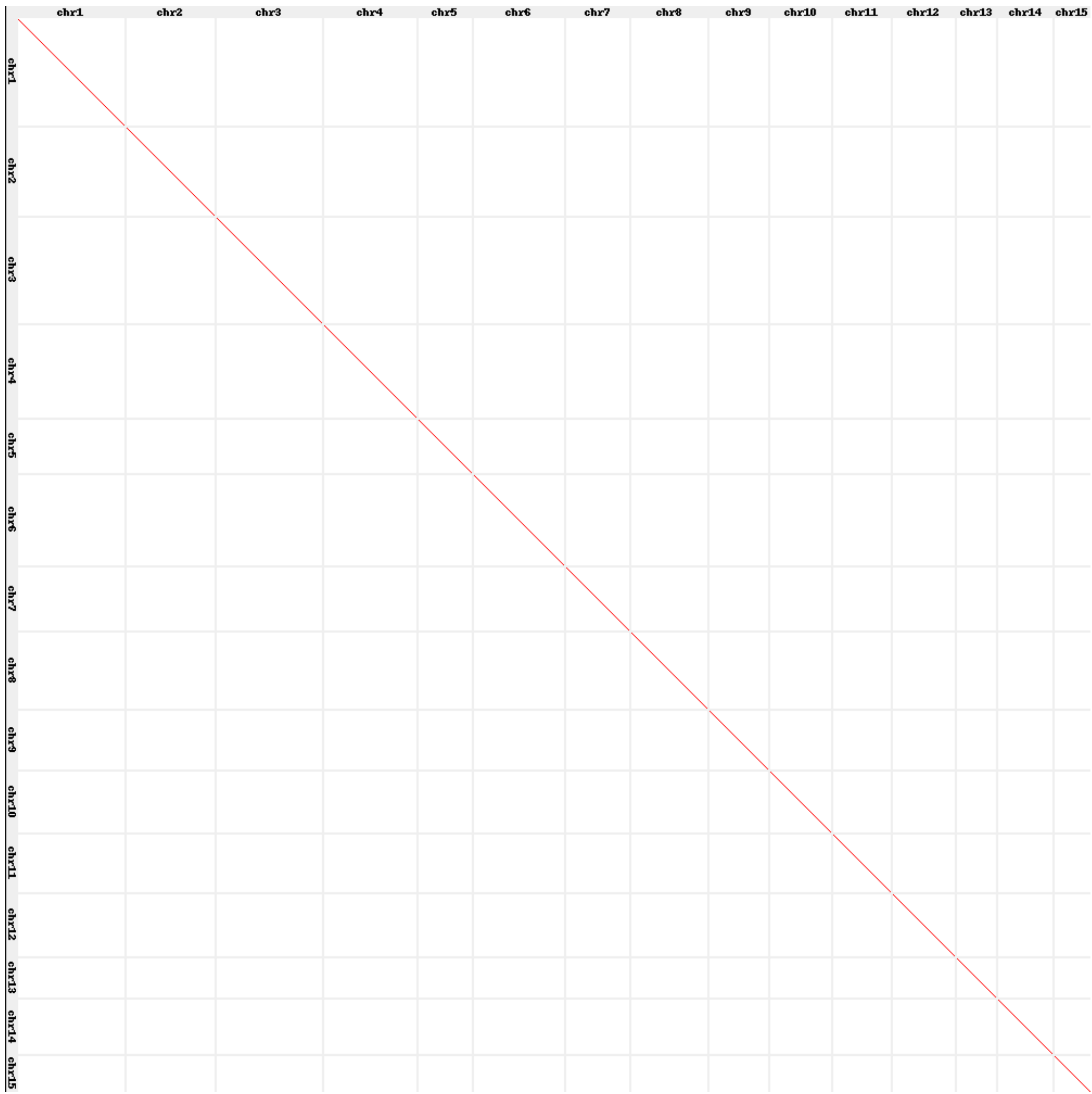
a**b**



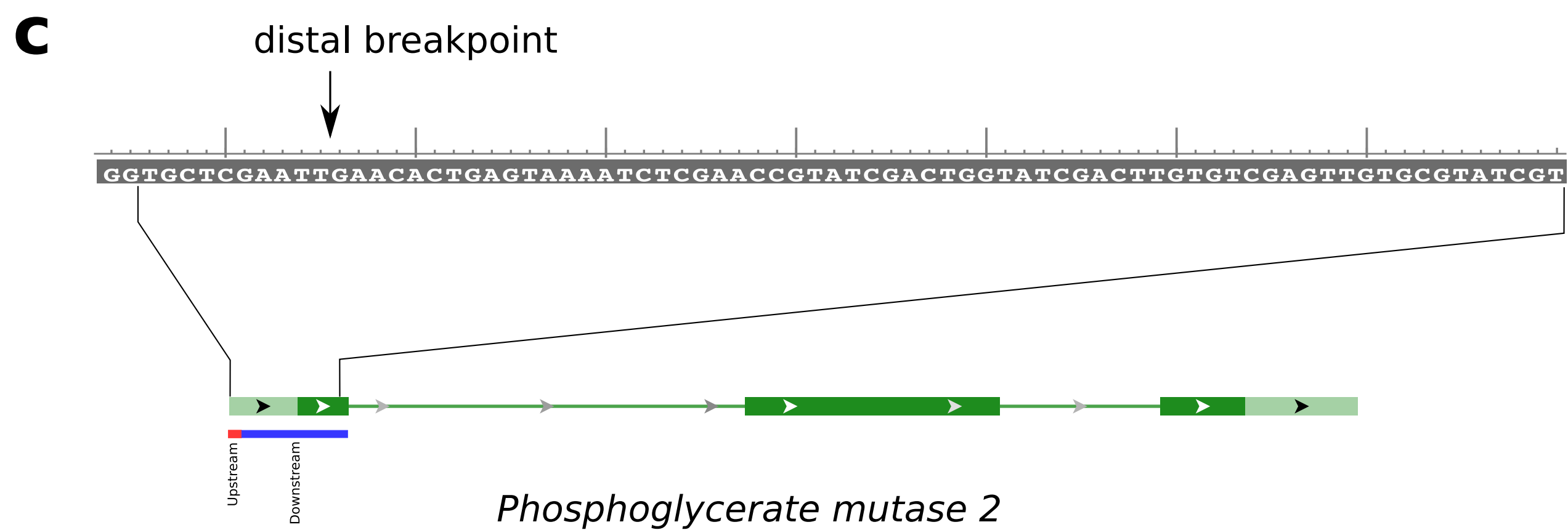
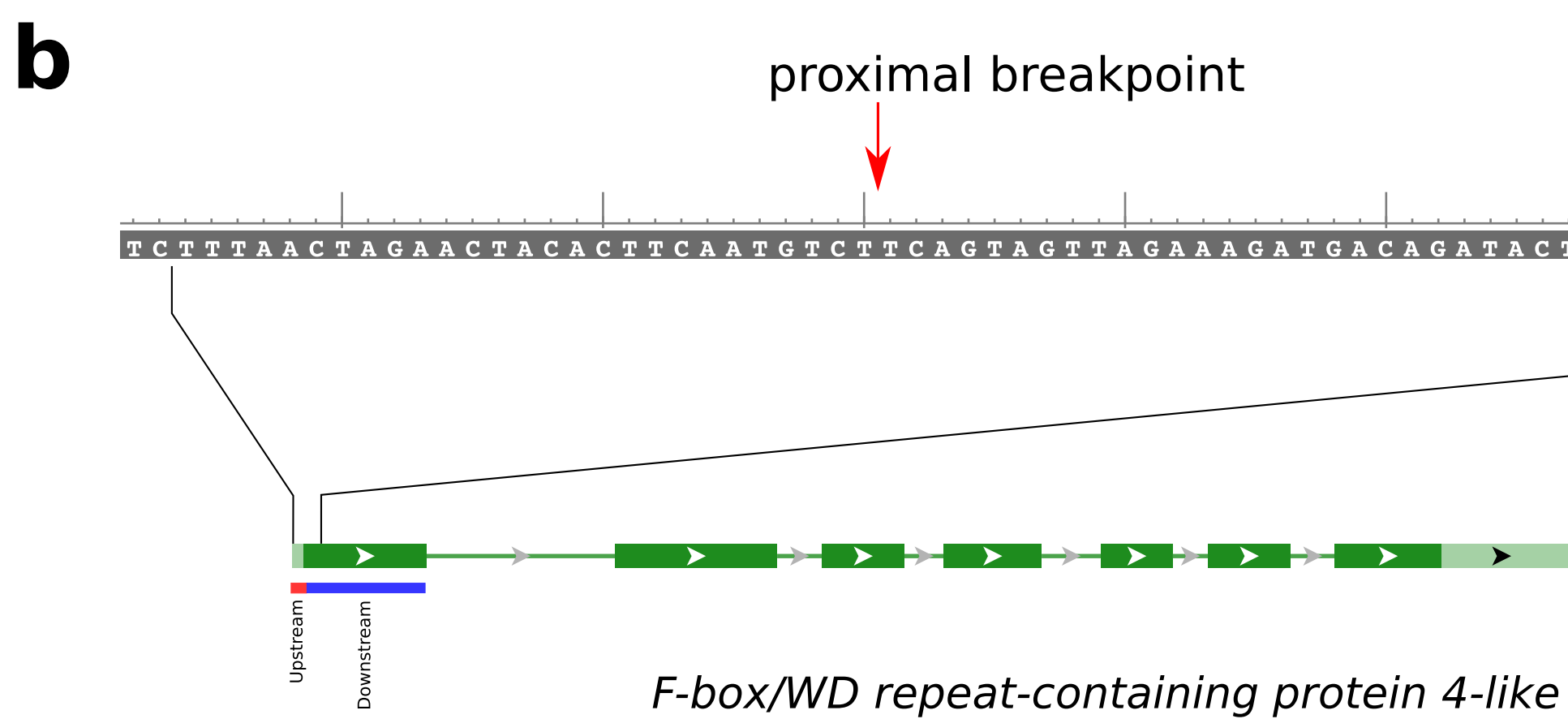
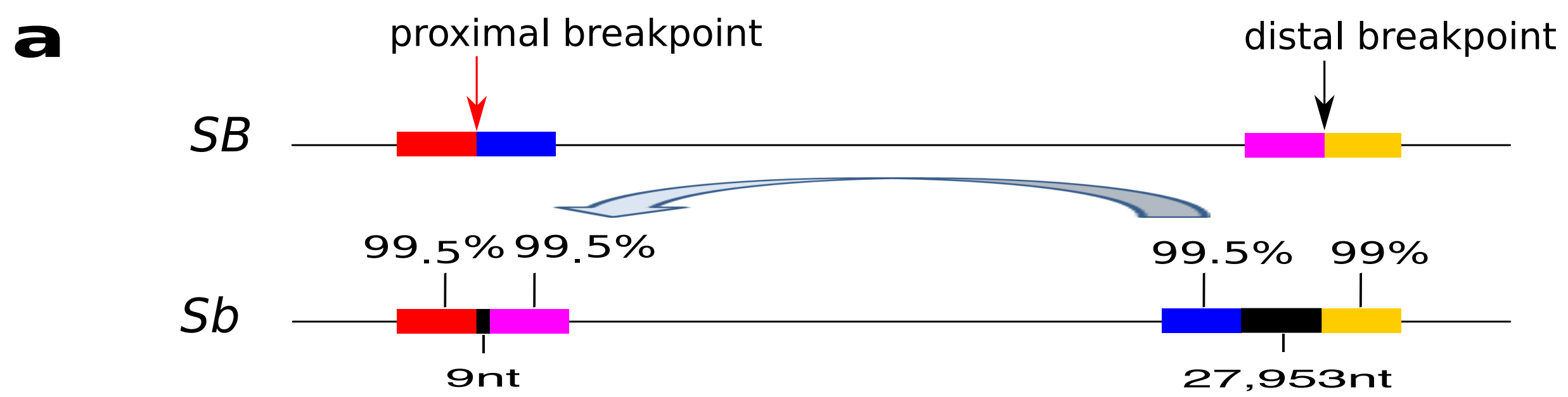
a*S. invicta-richteri-AdRX**S. macdonaghi-megergates-nr. interrupta***b**

SB male

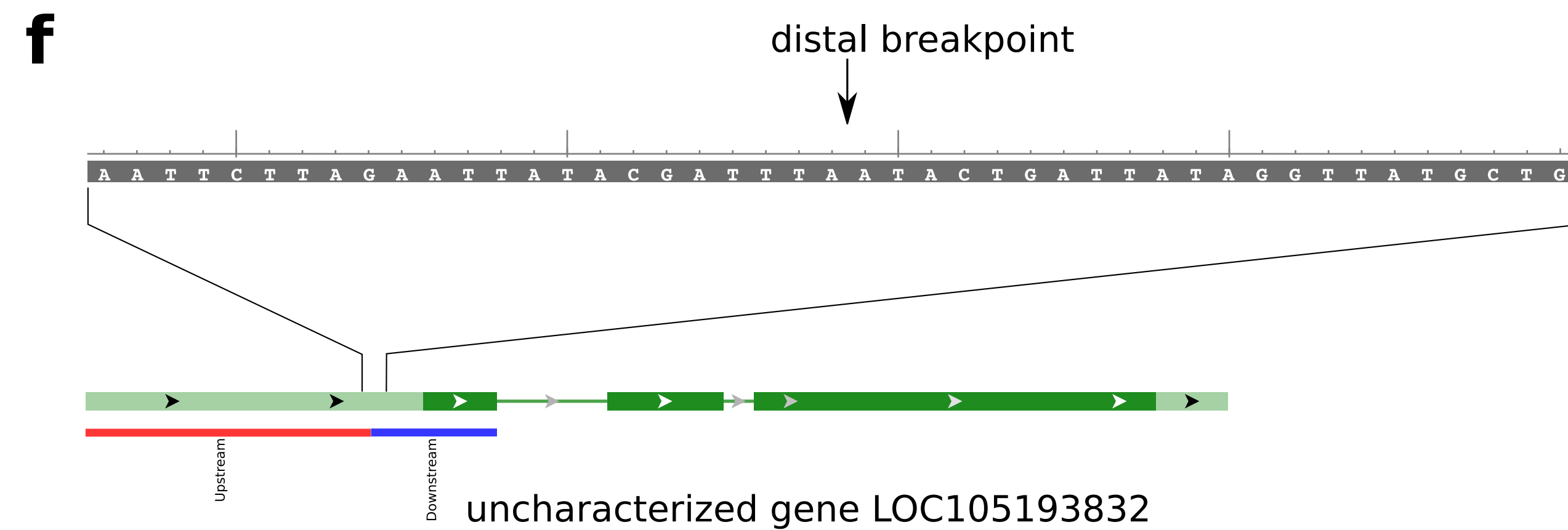
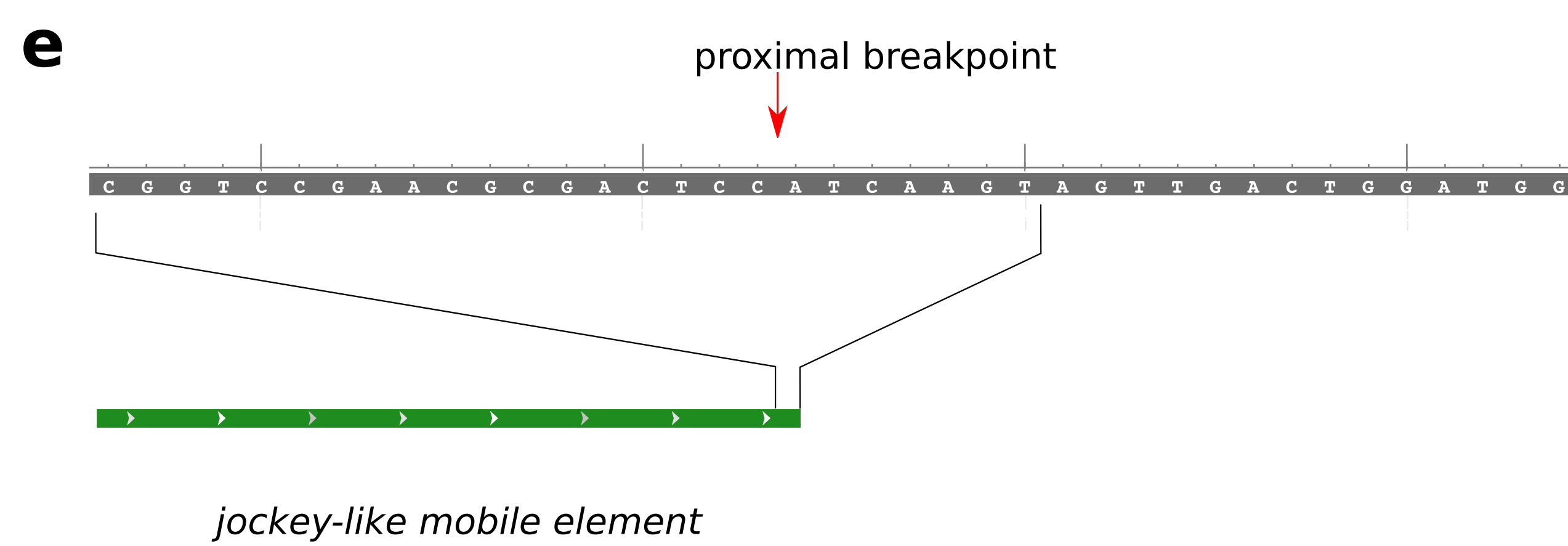
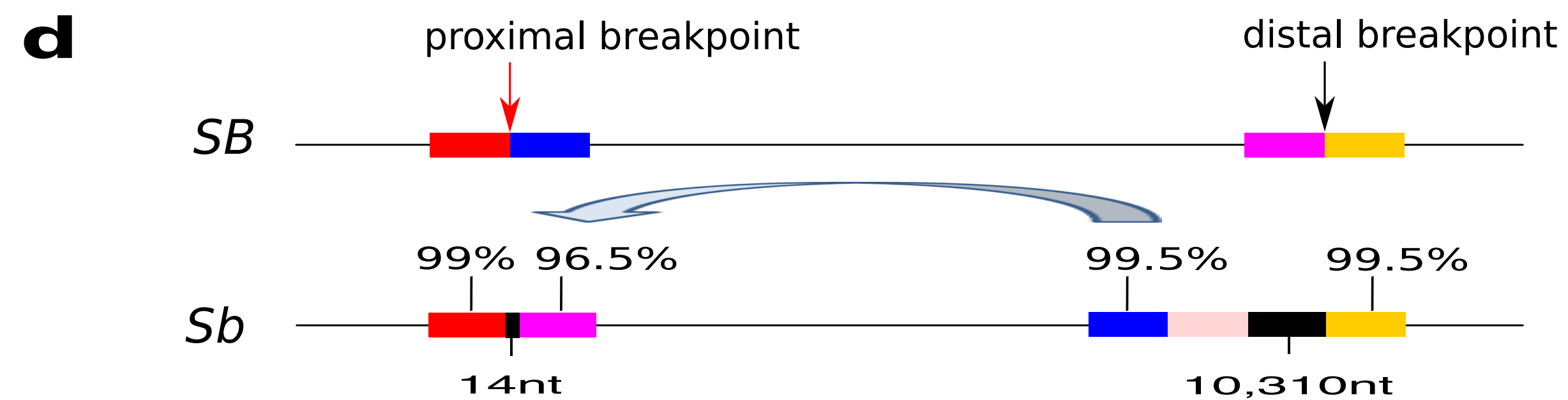
Sb male
qs



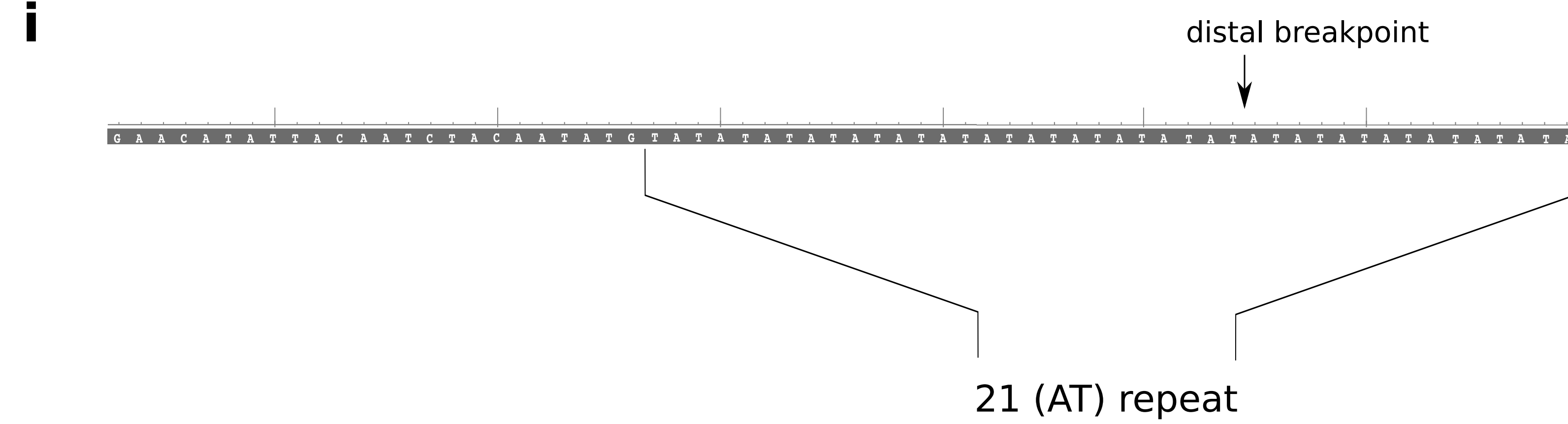
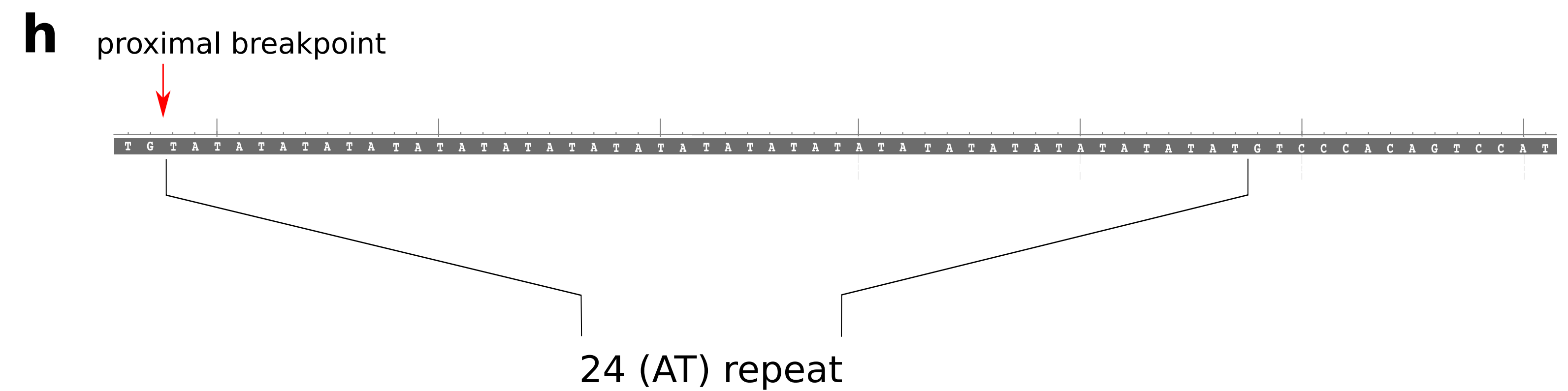
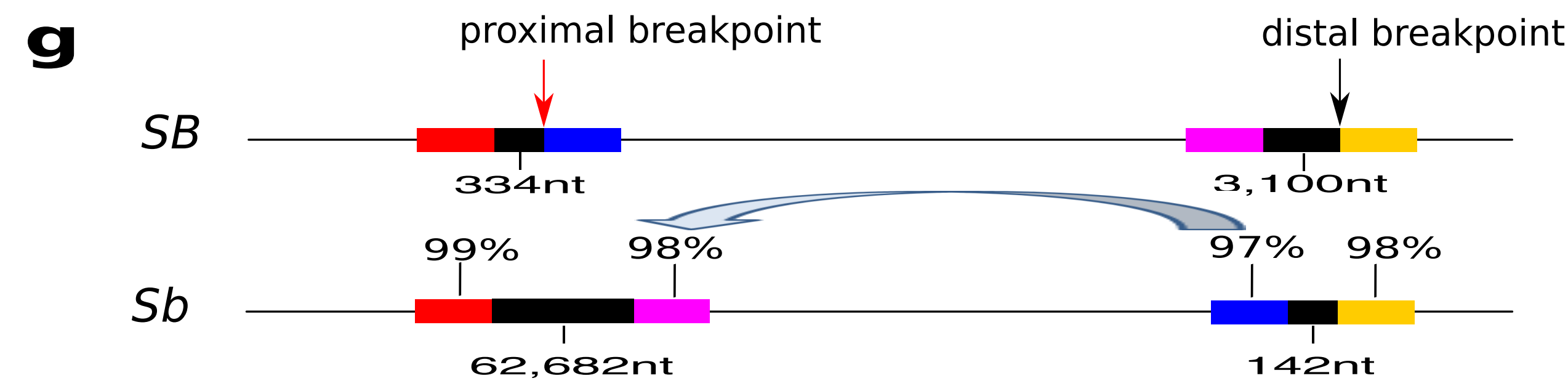
In(16)1



In(16)2



In(16)3



Phosphoglycerate mutase 2 (PGAM2)



F-box/WD repeat-containing protein 4-like (FBXW4)

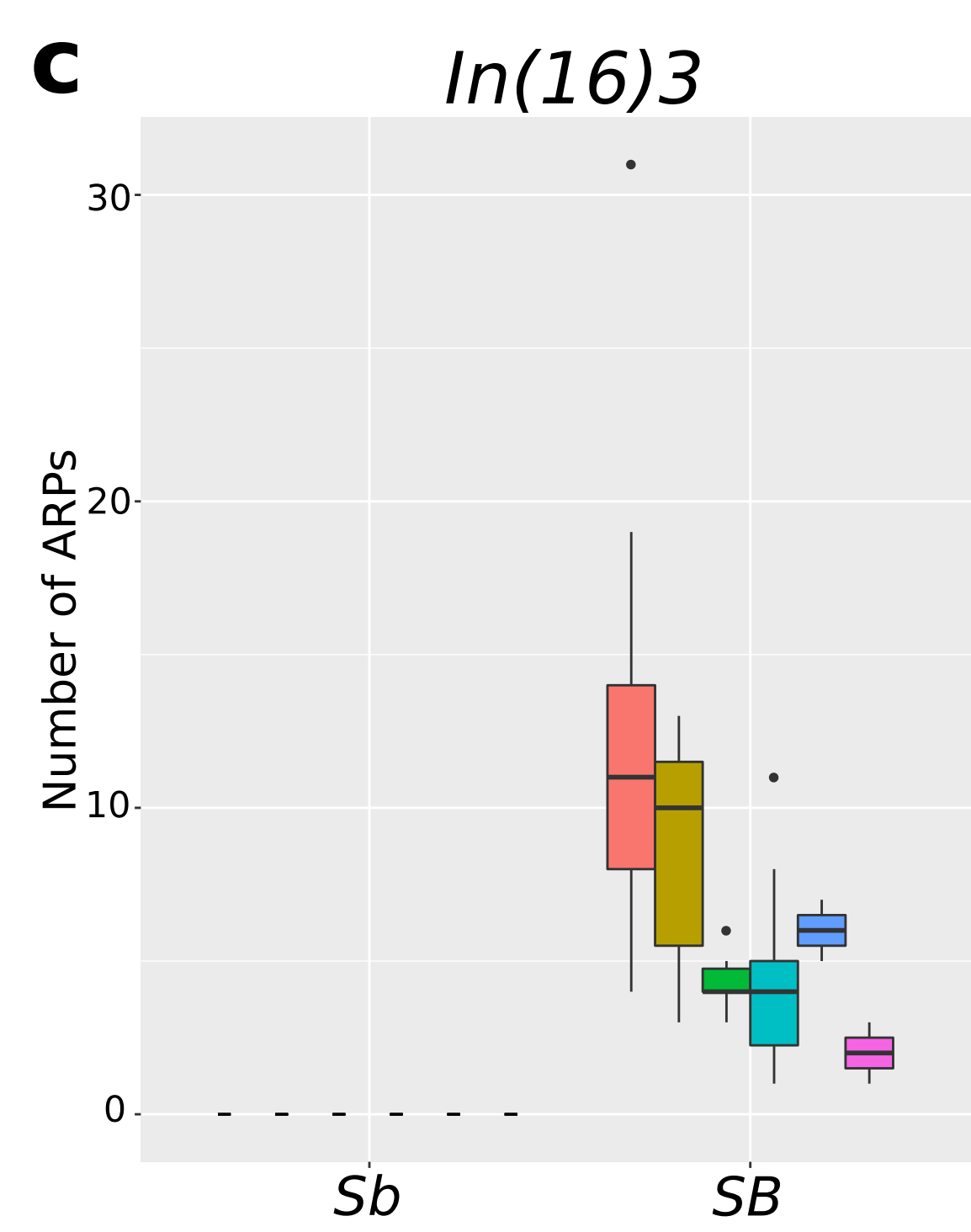
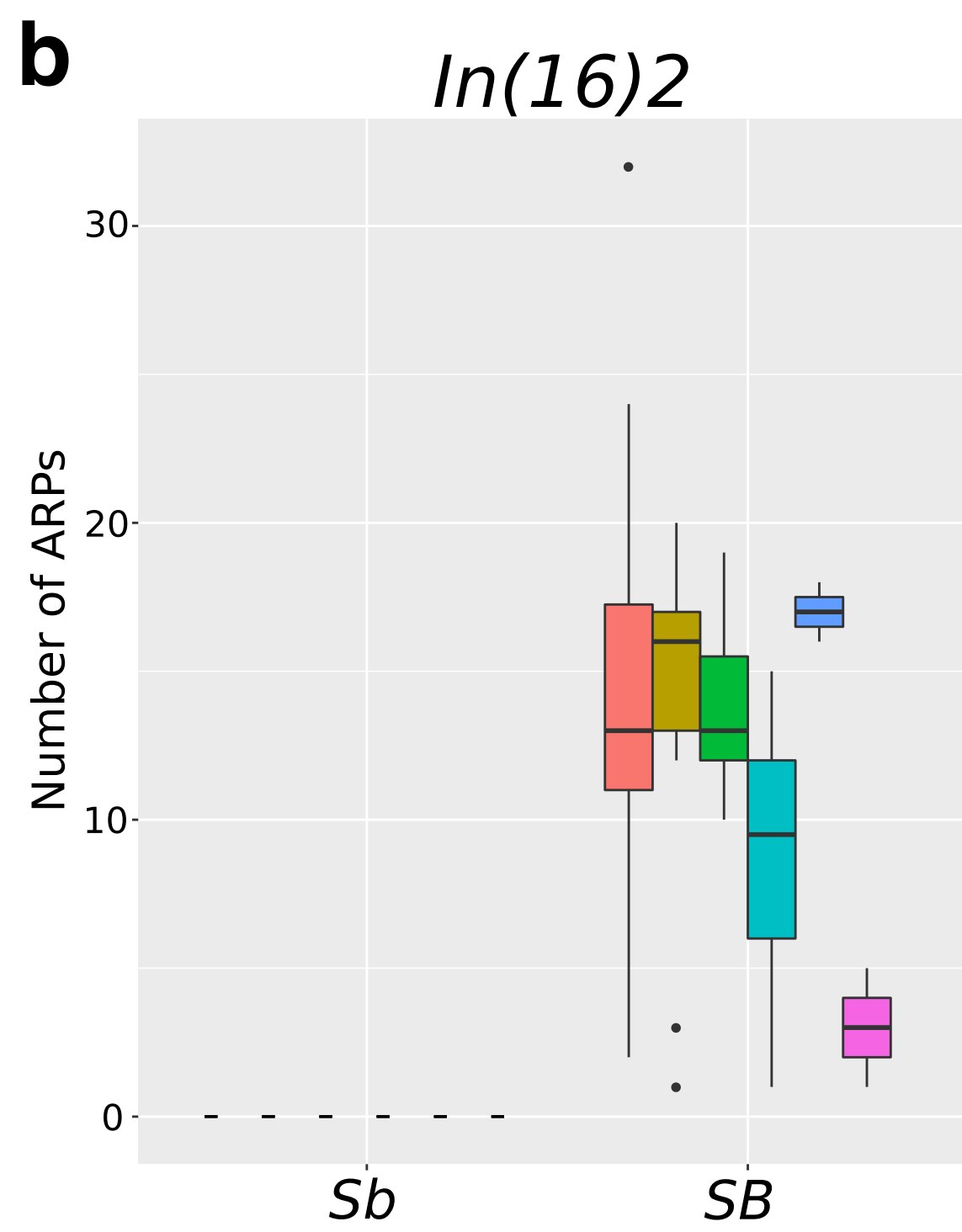
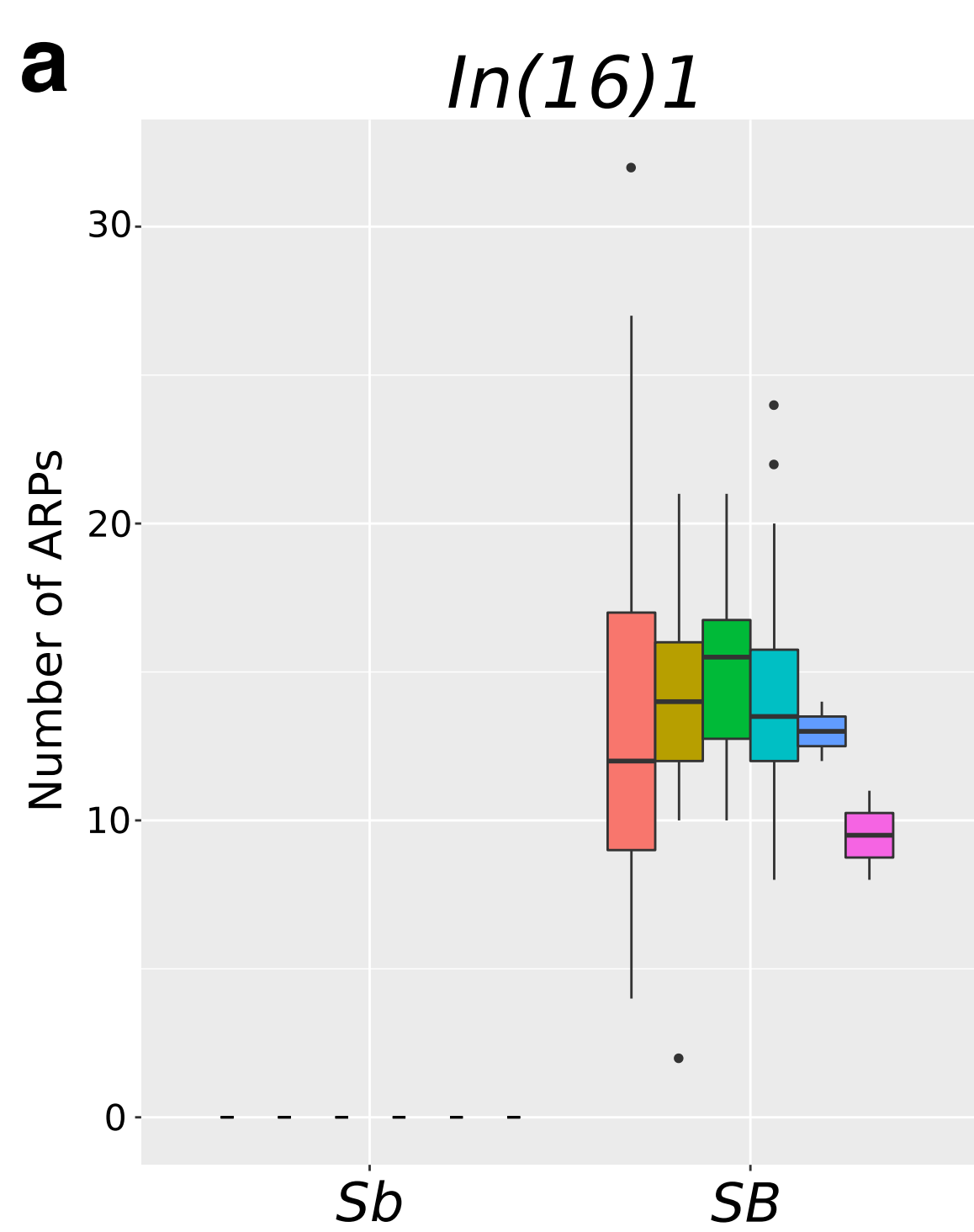


C

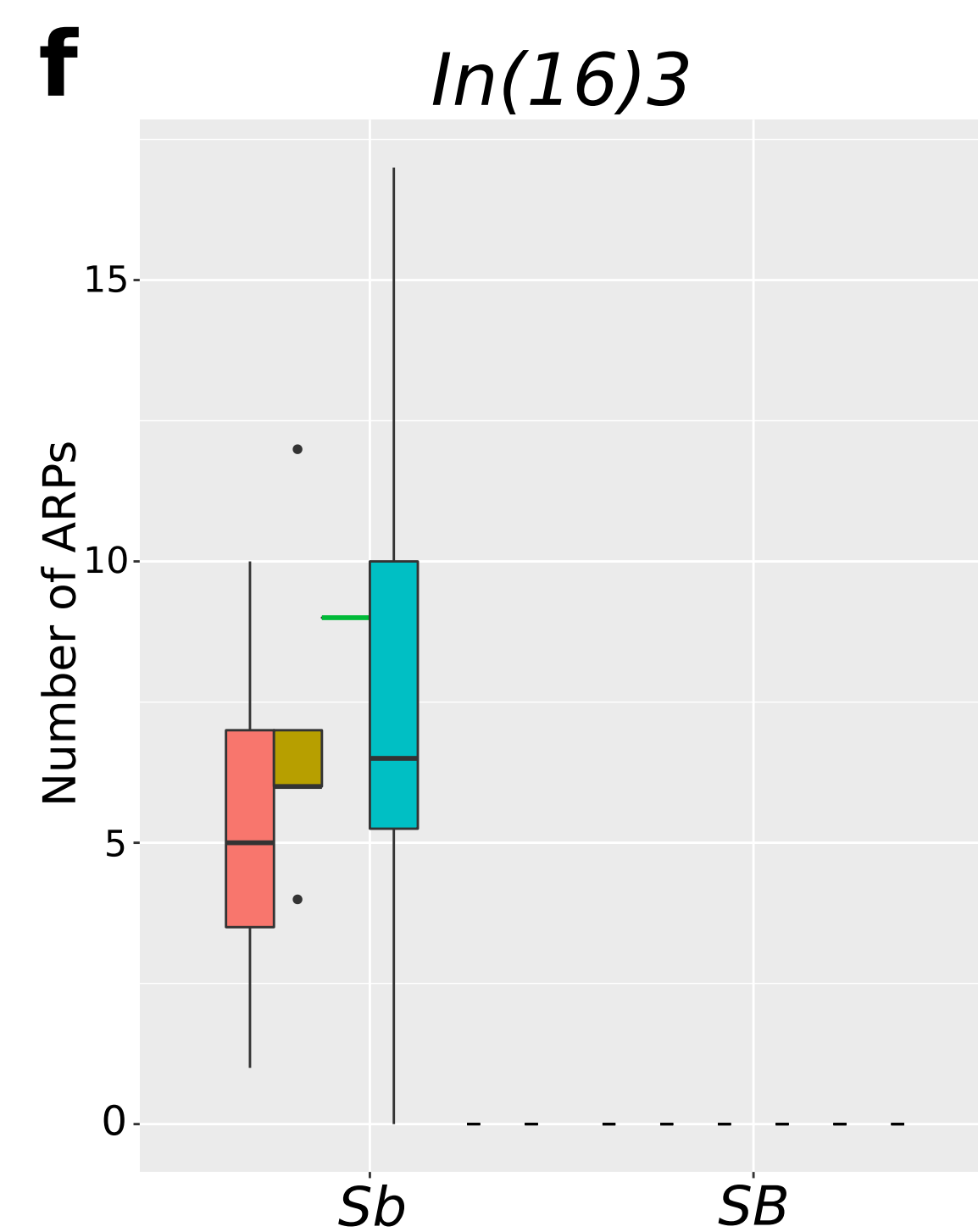
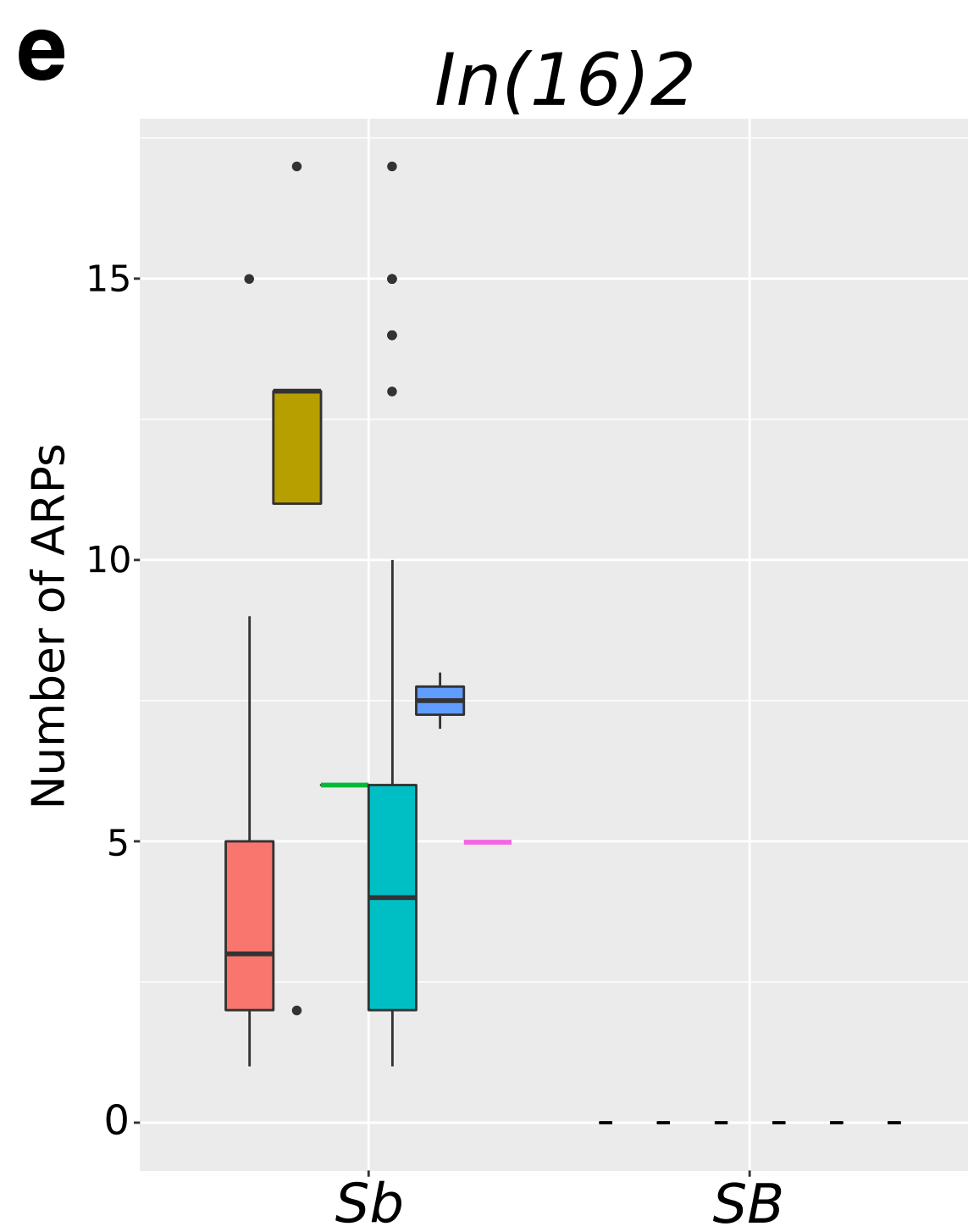
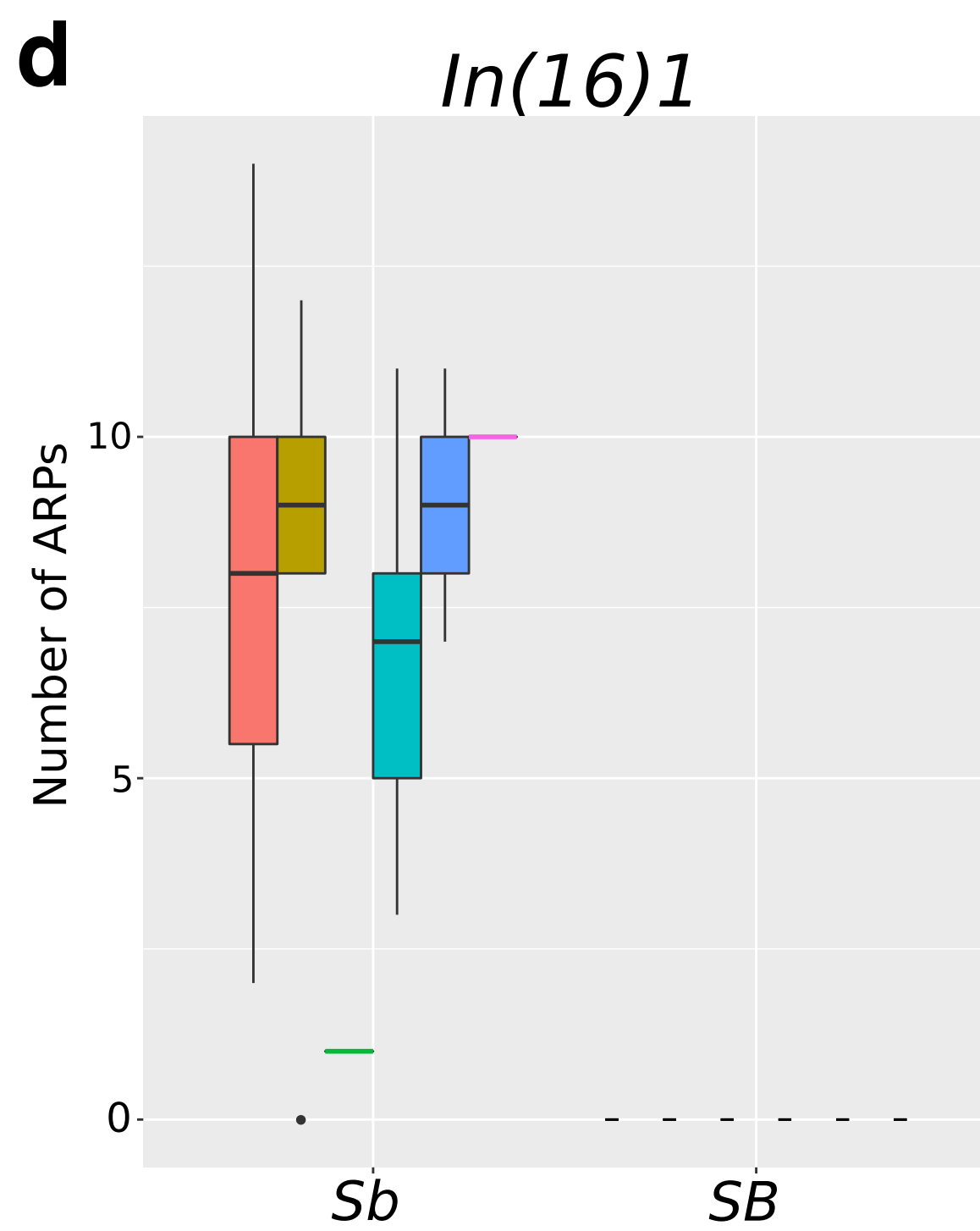
<i>Solenopsis invicta</i>		<i>Drosophila melanogaster</i>	Viability Effects of Gene Disruption (Flybase)	Substrates
PGAM2 (XP_011156752)	<i>ortholog*</i>	PGAM (CG1721)	Viable	
FBXW4 (XP_011164632)	<i>paralogs**</i>	<i>Ago</i> (CG15010)	Lethal	Trh, CycE, dMyc, Notch
		<i>Slimb</i> (CG3412)	Most are lethal	ARM, Ci, Cact, Dl, E2F, PER, PLK4, Rel
		<i>Fbw5</i> (CG9144)	Viable	Myc, trh, sima, CycE

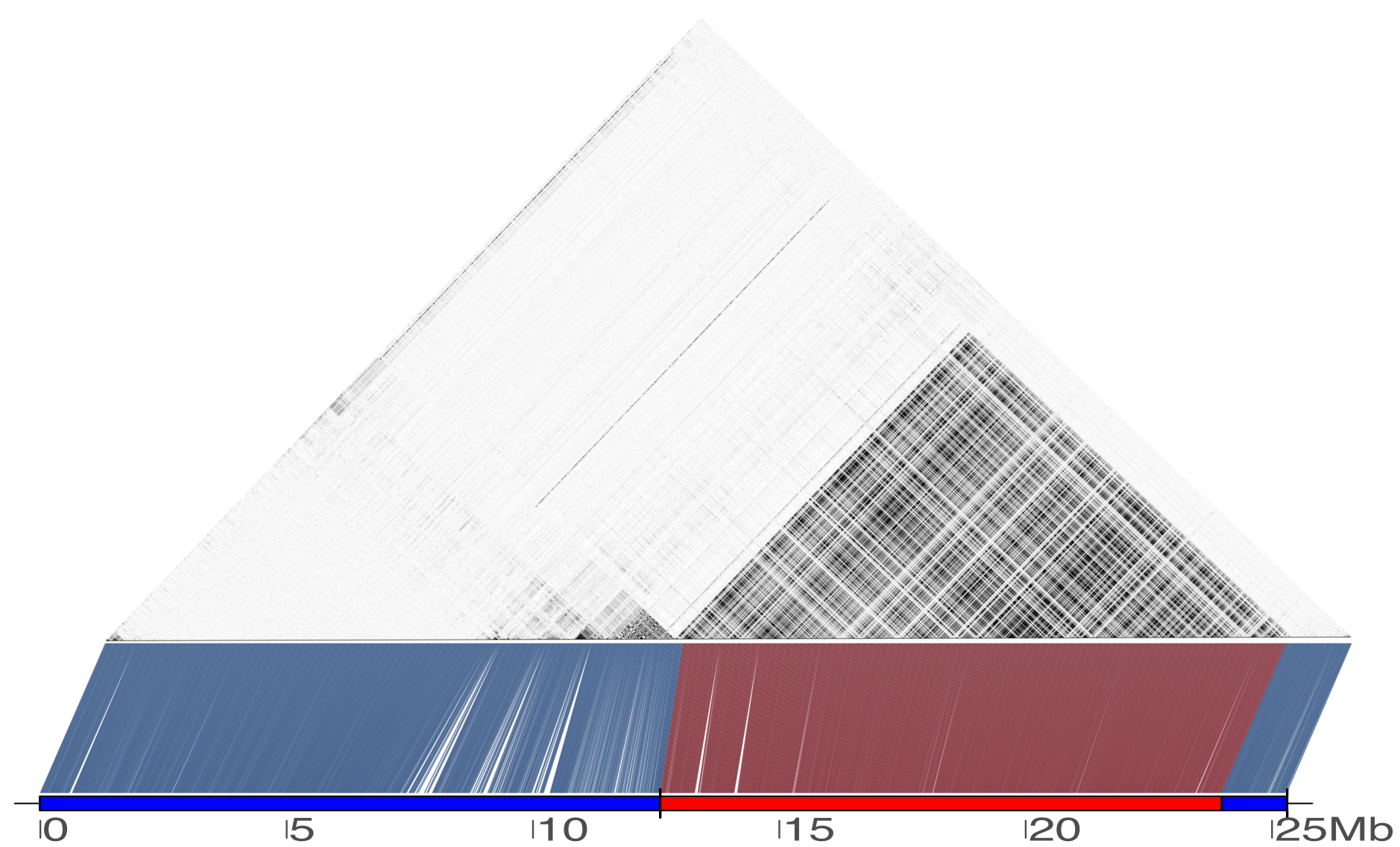
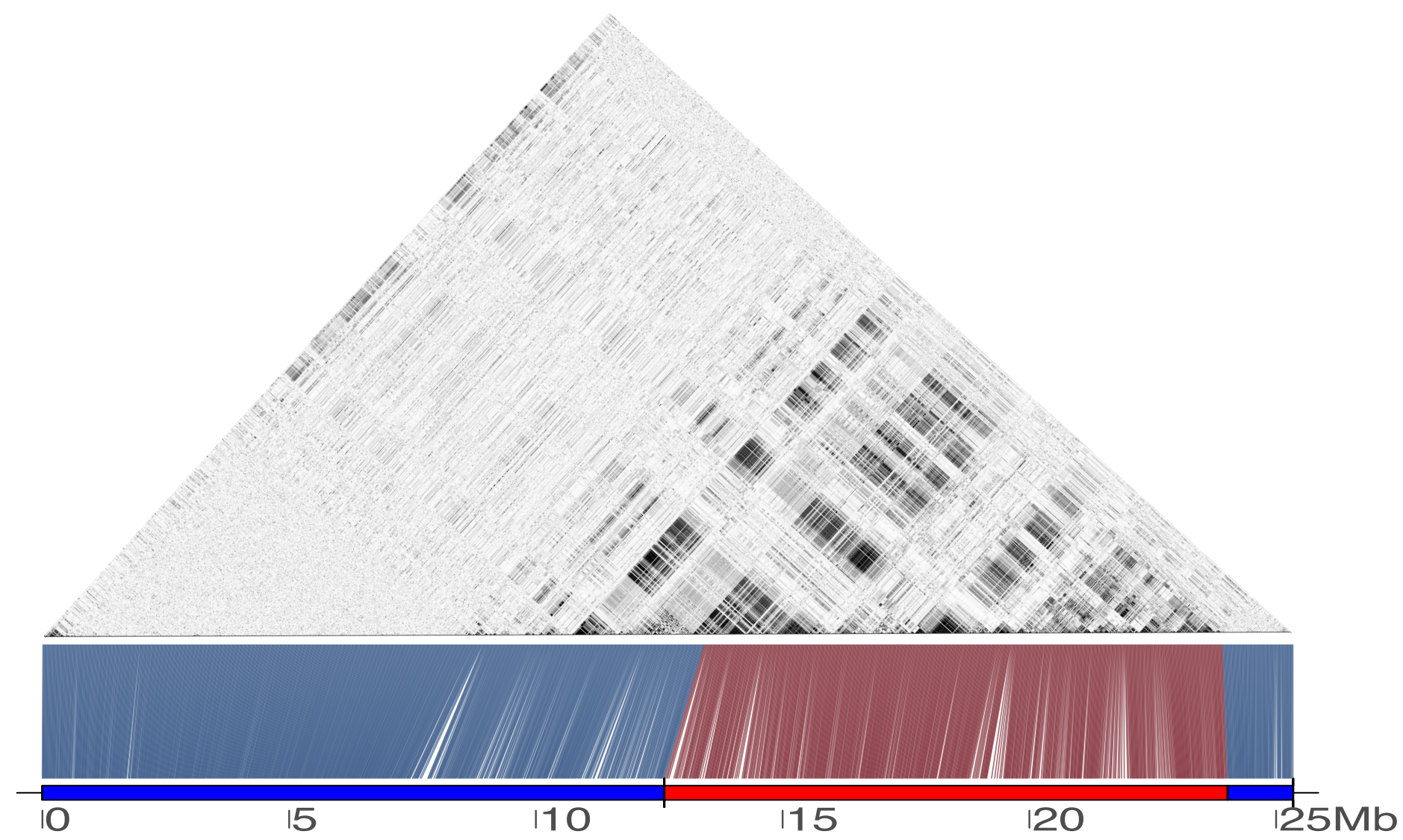
* Based on reciprocal best BLAST
**Based on the protein domains combination

Sb reference genome

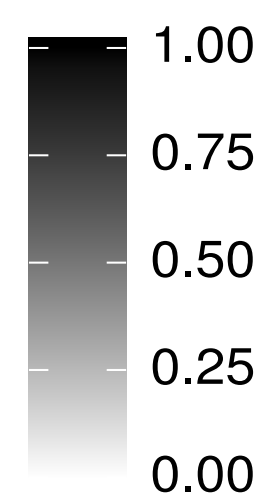
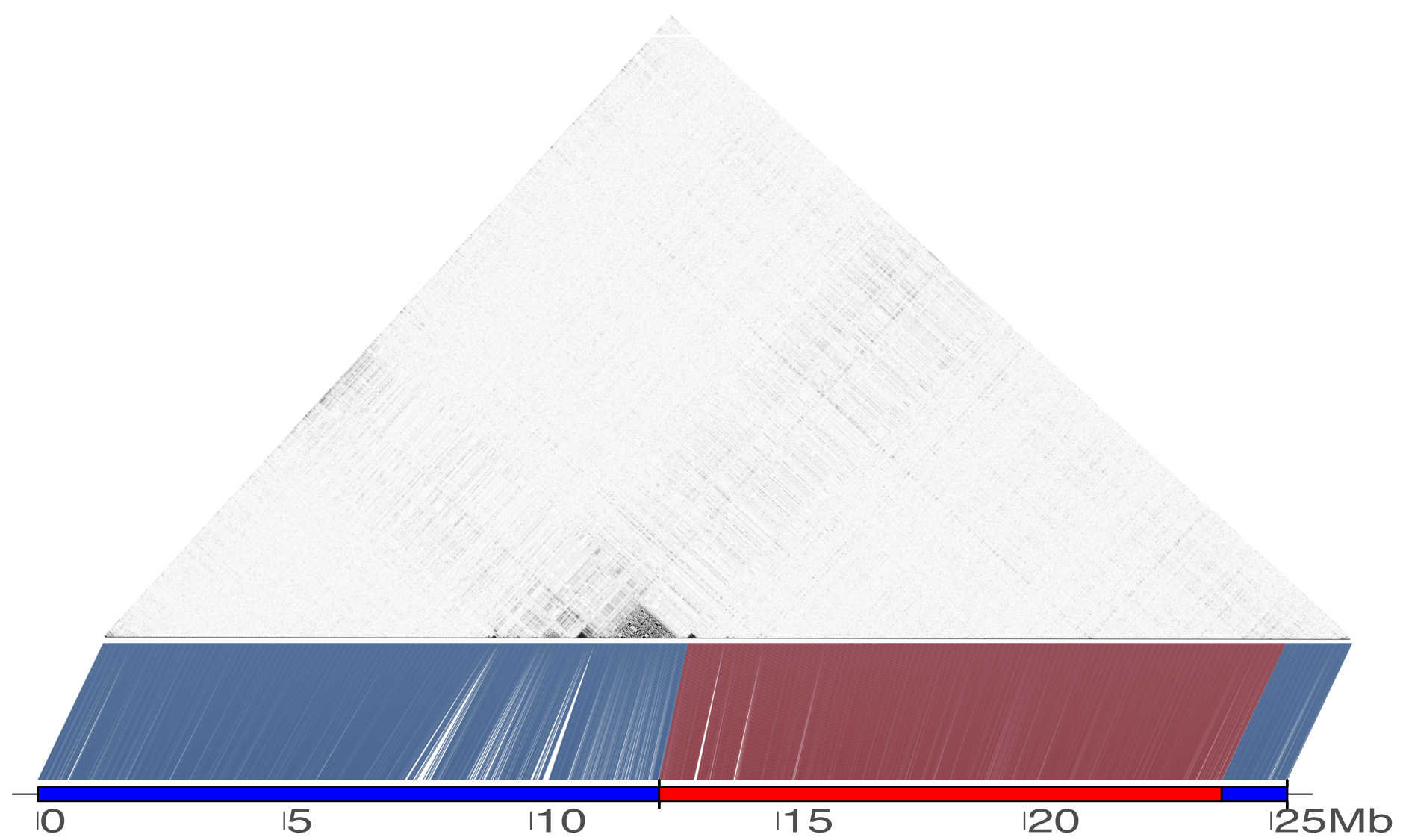


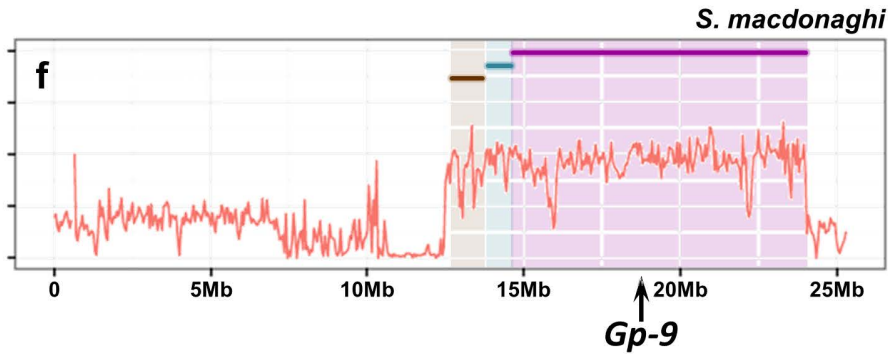
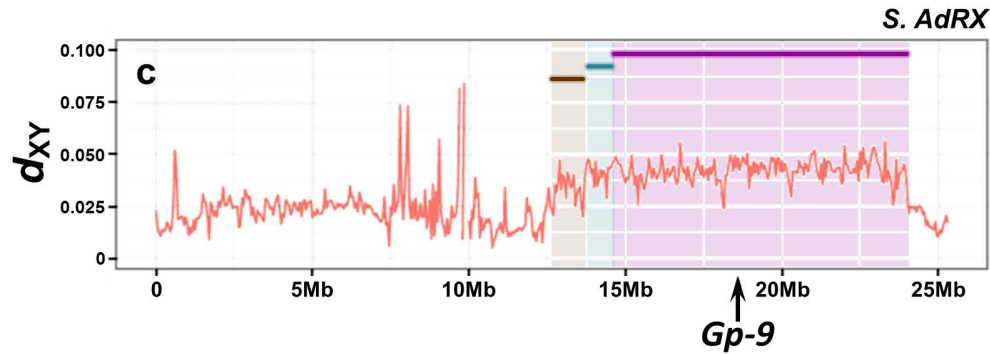
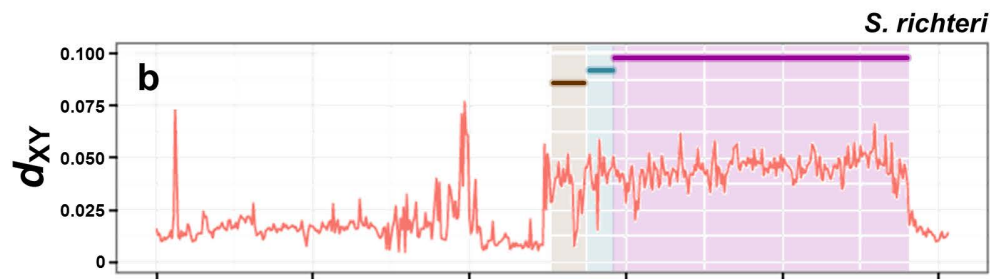
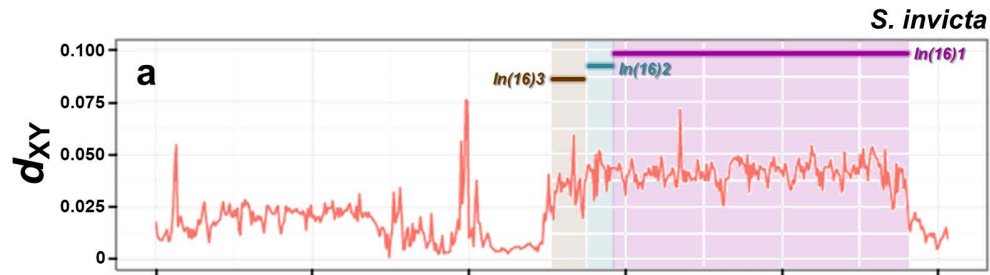
SB reference genome

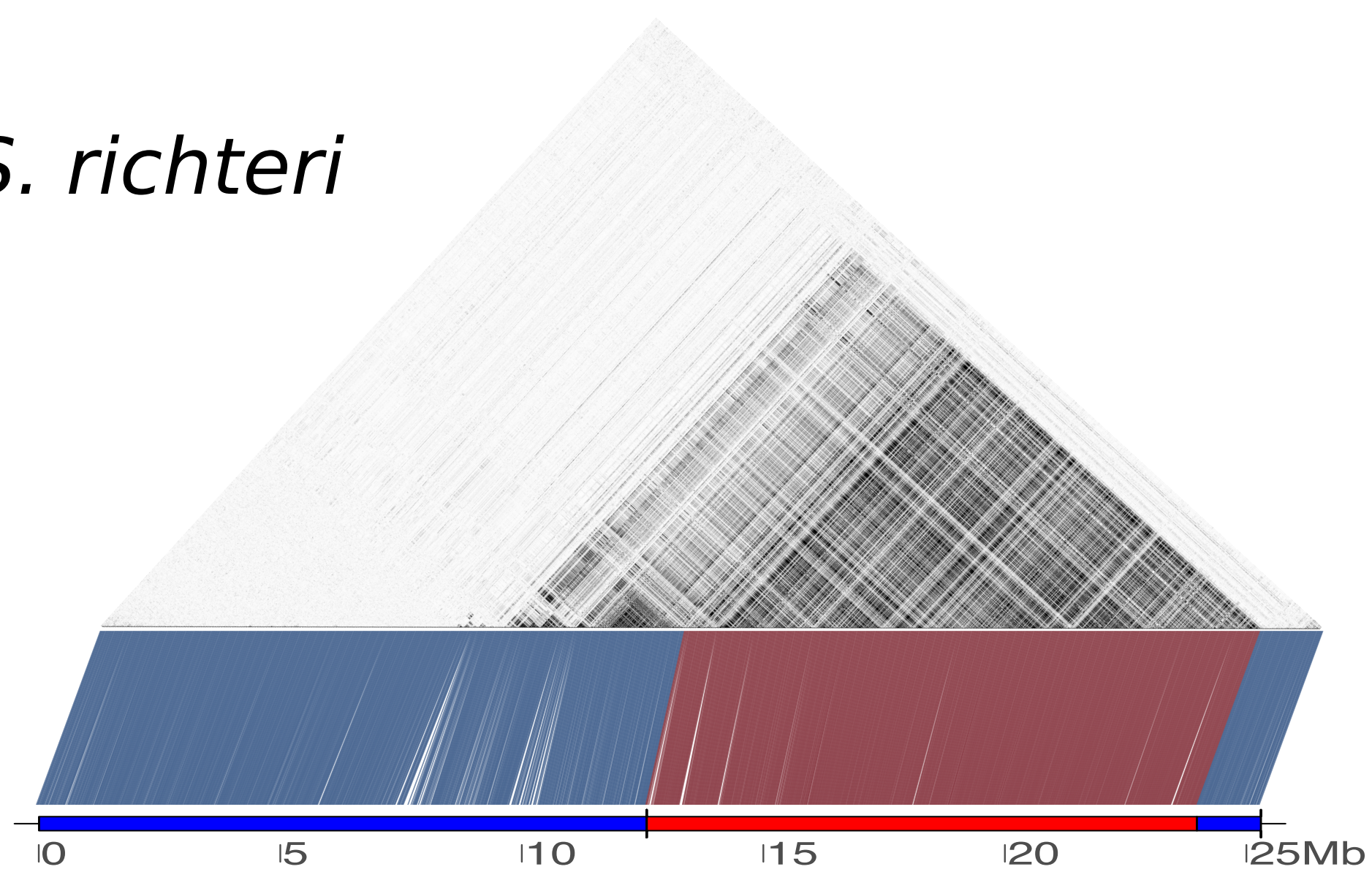
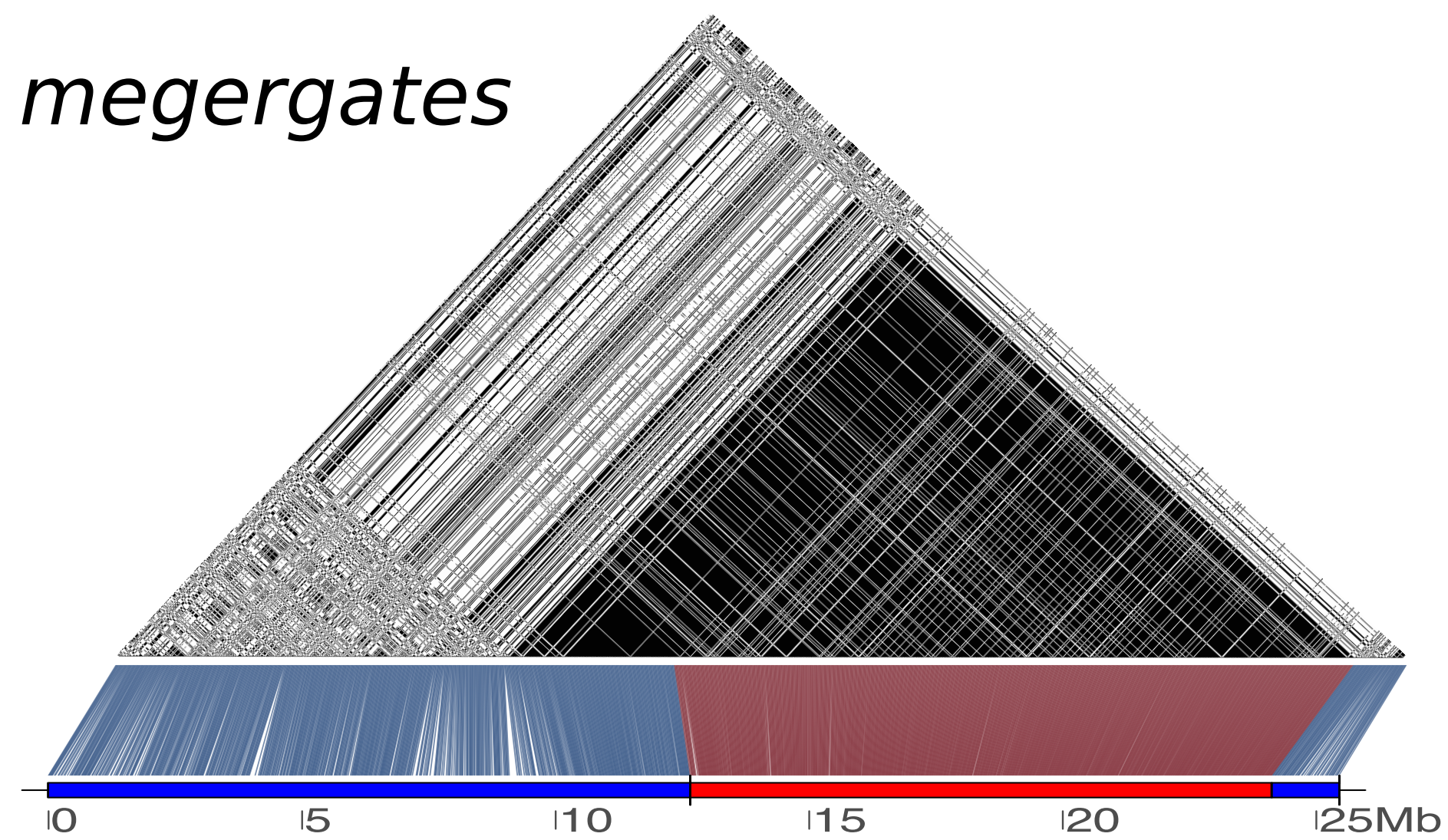
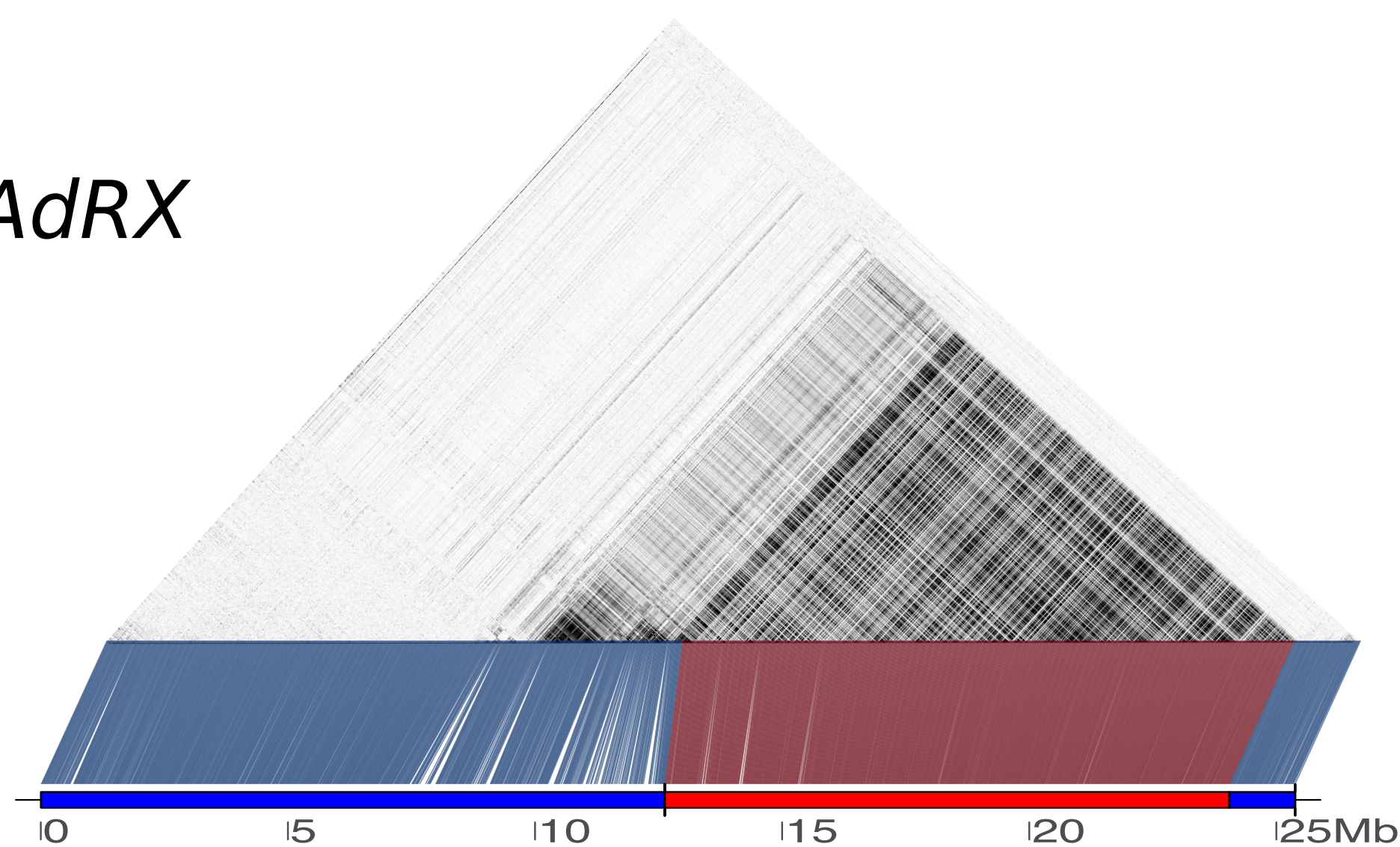
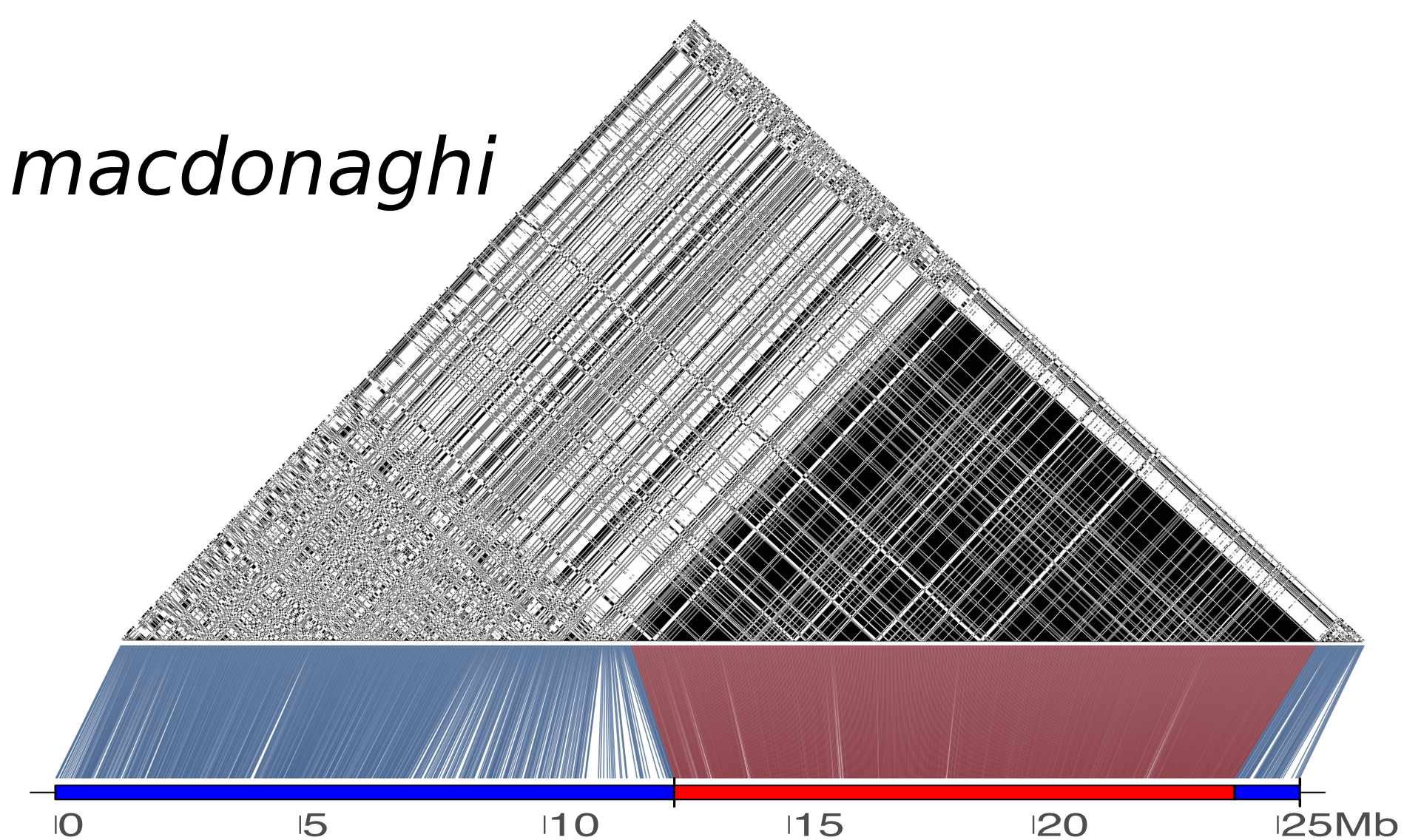
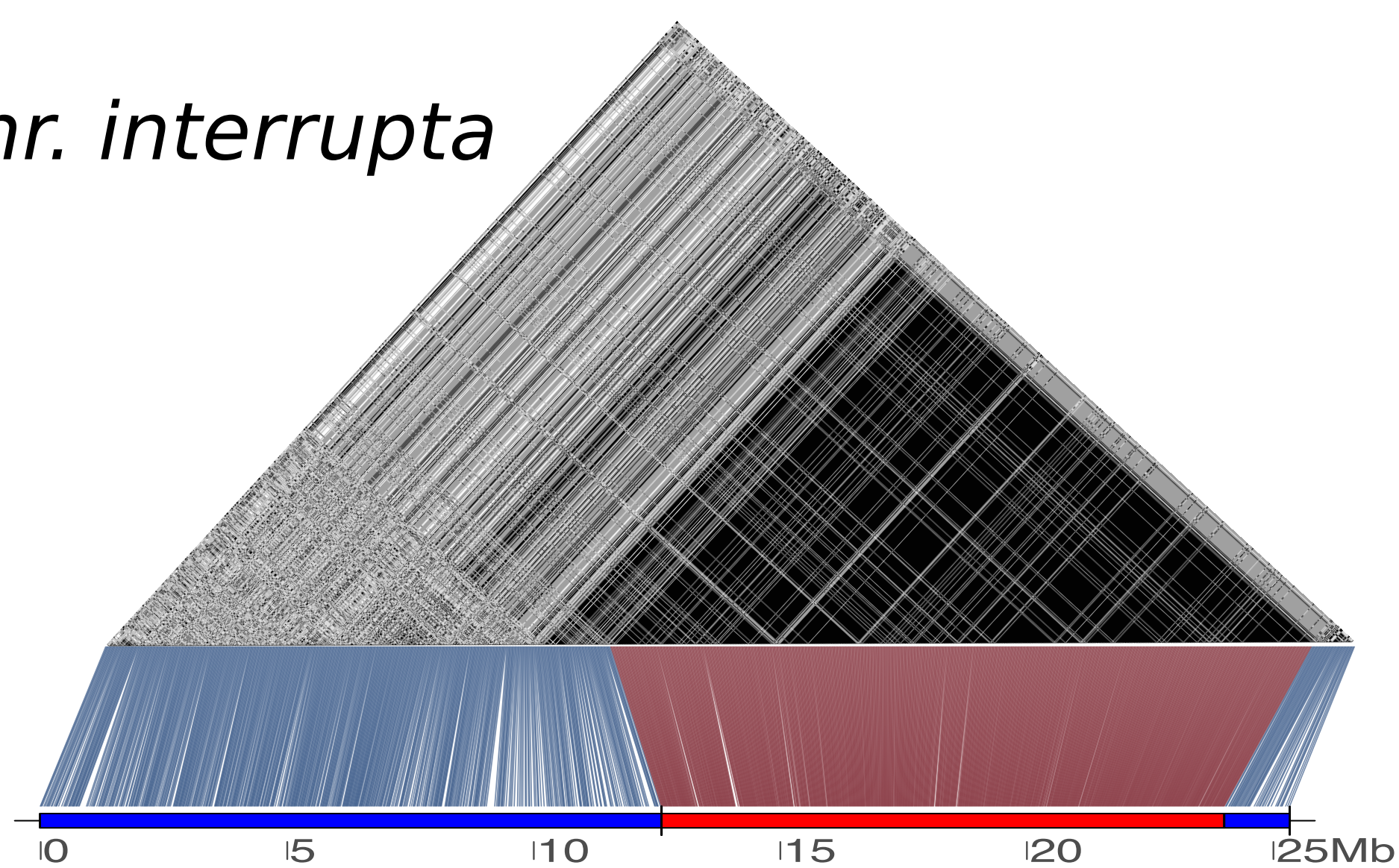
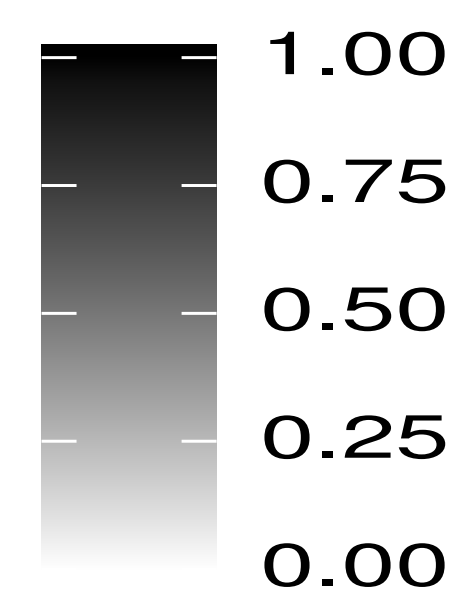


a**b**

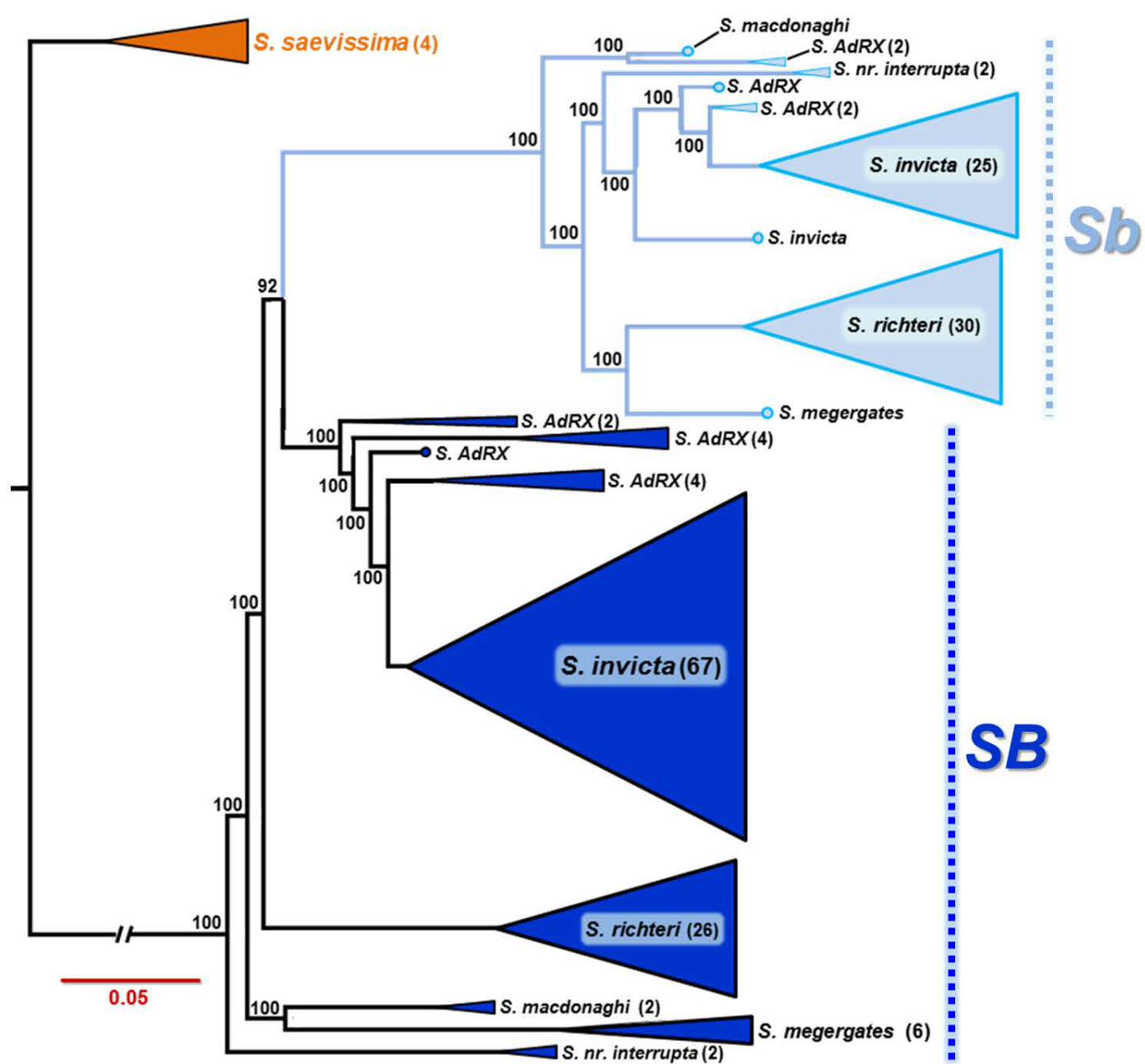
r^2 := gametic disequilibrium

**c**

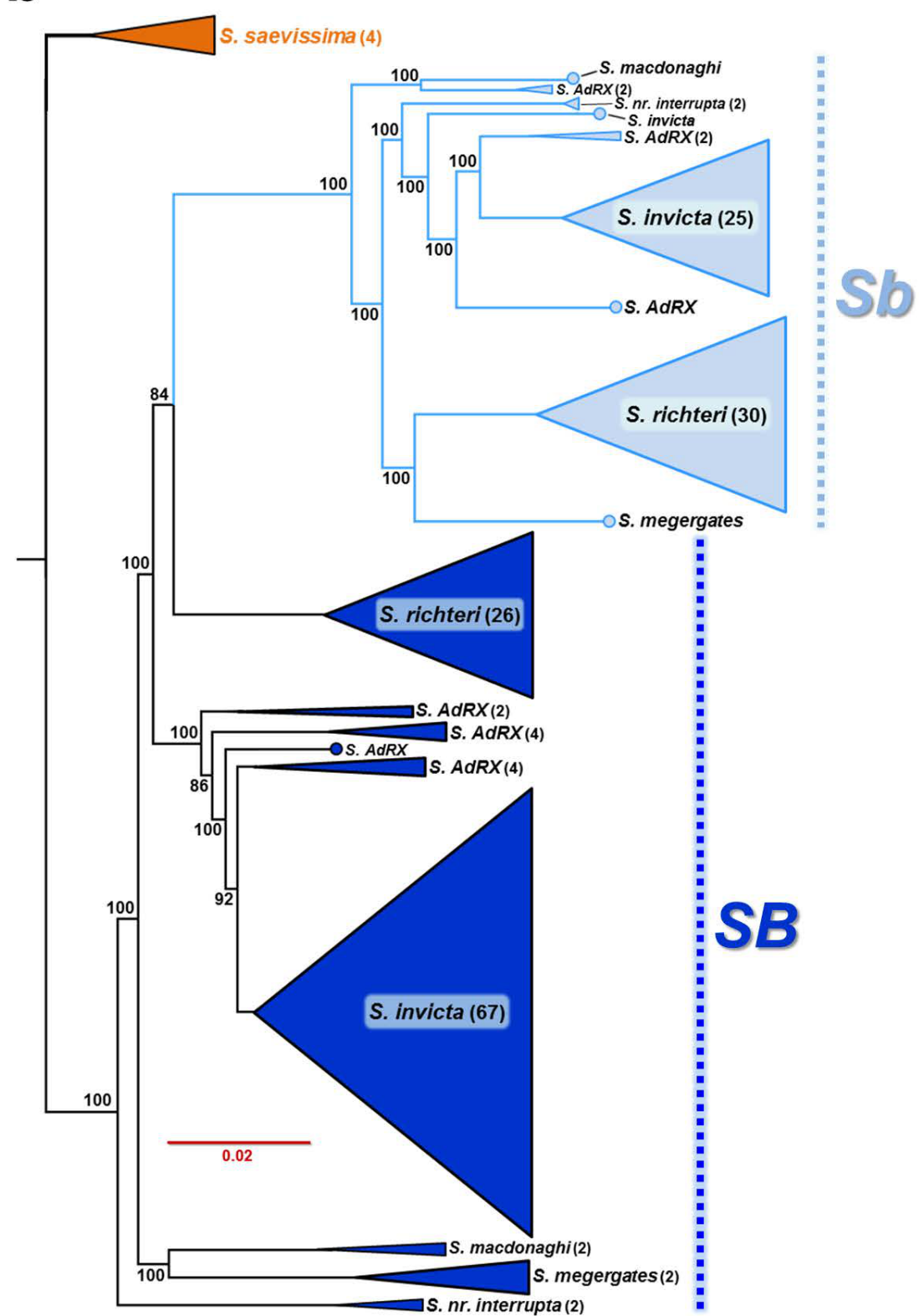


a*S. richteri***d***S. megergates***b***S. AdRX***e***S. macdonaghi***c***S.nr. interrupta* r^2 ; = gametic disequilibrium

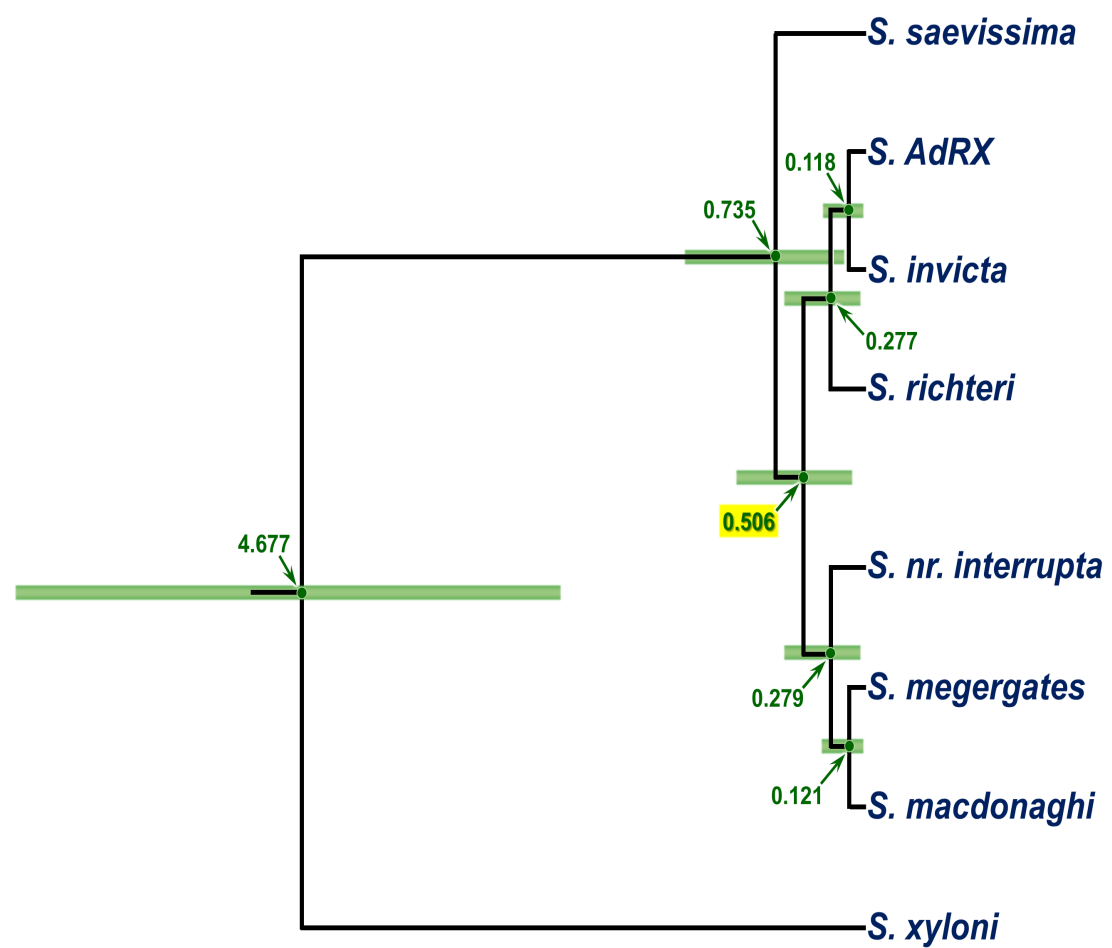
a

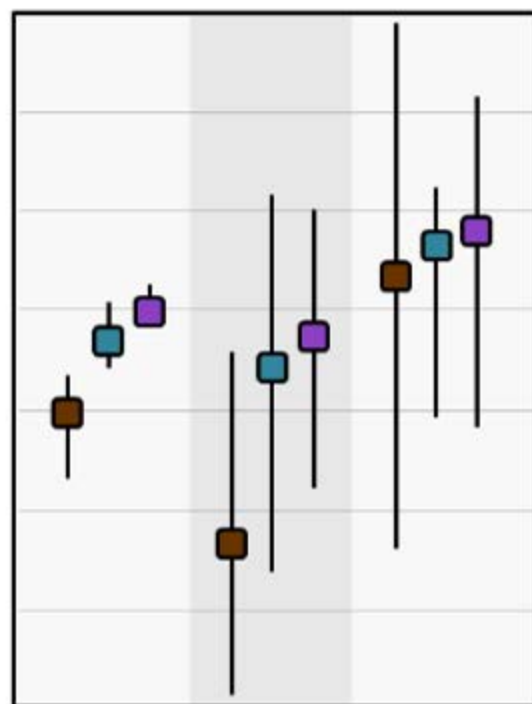
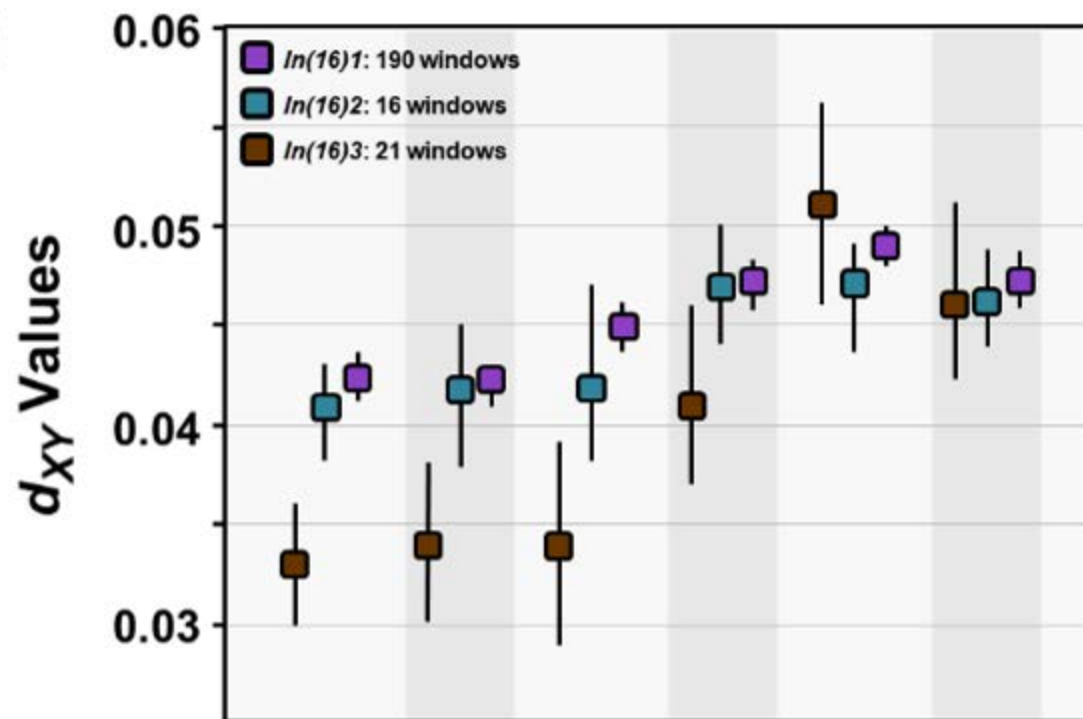


b



c



a**b**